Large Scale Fabrication of Field-Effect Devices based on *In Situ* Grown Carbon Nanotubes

Lorraine Rispal

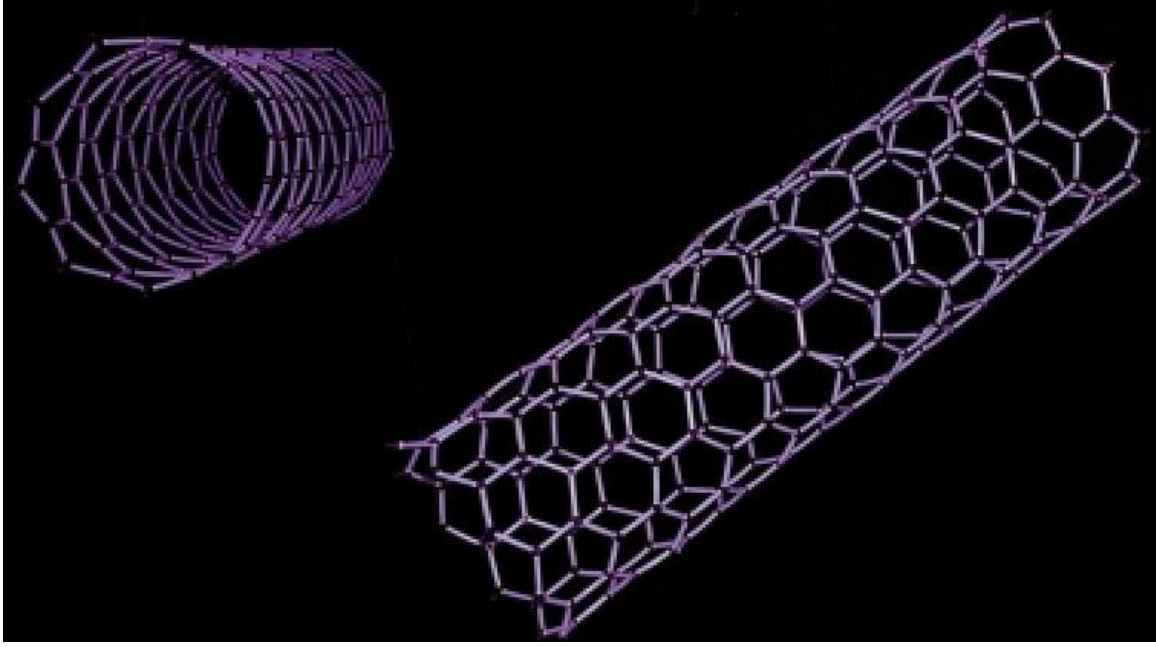

TECHNISCHE UNIVERSITÄT DARMSTADT

IHT Institut für Halbleitertechnik und Nanoelektronik

Large Scale Fabrication of Field-Effect Devices based on *In Situ* Grown Carbon Nanotubes

Vom Fachbereich Elektrotechnik und Informationstechnik
der Technischen Universität Darmstadt
zur Erlangung des akademischen Grades eines
Doktor-Ingenieurs (Dr.-Ing.)
genehmigte Dissertation

von

Dipl.-Ing. Lorraine Rispal

Geboren am 04.07.1980 in Paris (Frankreich)

Referent:	Prof. Dr. Udo Schwalke
Korreferent:	Prof. Dr. Wolfgang Krautschneider

Tag der Einreichung:	19.08.2009
Tag der mündlichen Prüfung:	19.11.2009

D 17
Darmstadt 2010

Erklärung zur Dissertation laut §9 PromO

Ich versichere hiermit, dass ich die vorliegende Dissertation allein und nur unter Verwendung der angegebenen Literatur verfasst habe. Die Arbeit hat bisher noch nicht zu Prüfungszwecken gedient.

Darmstadt, den 19.08.2009

_____

Lorraine Rispal

Danksagung

Die vorliegende Arbeit entstand während meiner Tätigkeit als wissenschaftliche Mitarbeiterin am Institut für Halbleitertechnik (IHT) der Technischen Universität Darmstadt.

Mein besonderer Dank gilt meinem Doktorvater, Herrn Prof. Dr. Udo Schwalke, zuerst für die Möglichkeit, fünf Jahre spannende Forschung in der Nanoelektronik durchführen zu können. Außerdem für das Vertrauen in meine Arbeit, die wissenschaftliche und moralische Unterstützung und die vielen Gespräche, die das Thema nach vorne gebracht haben, sowie die richtigen Impulse zur richtigen Zeit, die Unterstützung während der Phase des Dissertationsschreibens, und schließlich auch für die Möglichkeit, meine Arbeit in internationalen Konferenzen zu zeigen und dadurch Anregungen und neue Ideen zu sammeln.

Herrn Prof. Dr. Wolfgang Krautschneider danke ich für das Interesse an der Arbeit und die Übernahme der Korreferats.

Ein spezieller Dank gilt Herrn Prof. Dr. Hans Strack, der meine Zwischenfinanzierung übernommen und mir dadurch die Gelegenheit gegeben hat, das spannende Thema meiner Doktorarbeit zu vertiefen.

Allen Kolleginnen und Kollegen am IHT möchte ich für die vielfältige Unterstützung während der Arbeit, die unterhaltsamen Gespräche sowie das angenehme Arbeitsklima danken. Insbesondere möchte ich mich bei Gisela Heß, Gudrun Müller und Gerhard Tzschöckel sehr herzlich für die fröhliche und freundschaftliche Frühstücks- und Mittagspause der letzten Jahre bedanken, in der sie mir vieles über die deutsche Kultur, insbesondere kulinarisch, vermittelt haben.

Weiterhin möchte ich mich bei den Studenten bedanken, die mit ihren Studienarbeiten zum Gelingen dieser Arbeit beigetragen haben.

Schließlich danke ich ganz herzlich meinen Eltern und Björn für ihre Unterstützung. *Enfin je voudrais remercier mes parents et Björn pour leur soutien.*

Abstract

Since the first integrated circuits in the late 1960's, a constant improvement of their performances could be reached by scaling down the metal oxide semiconductor field-effect transistors (MOSFETs). However, downscaling of MOS transistors has reached its physical limits: the gate oxide is only composed of a few atomic layers, leakage currents are increasing and the short channel effects degrade device properties. These are the reasons why new integration concepts need to be developed to replace silicon based nanoelectronics. One of these concepts involves carbon nanotube field-effect transistors (CNTFETs). The active part of CNTFETs, i.e., the channel, is formed by a semiconducting single-walled carbon nanotube (SWNT), the growth of which represents one of the great challenges of CNT technology. Most publications on this topic report on a separate growth of nanotubes, either by arc discharge or laser ablation. These methods are not suitable for the fabrication of a large number of devices because they often require complicated manipulation and assembly after growth. Due to the improper growth method, state-of-the-art CNTFETs are mostly only single prototypes. Data on fabrication process suitability (e.g. time, costs), device reproducibility and reliability or yield are not available. However, a candidate for replacing MOSFET should not only have better performances but it should also be possible to produce it in large quantities to allow integration on a very large scale, i.e., billions of transistors on one wafer. Improving the knowledge of the scientific community on the feasibility of large scale fabrication of carbon nanotube devices constitutes the major motivation of this PhD work.

The primary aim of this PhD work is the development of a CMOS compatible fabrication process for CNTFETs which allows large scale production of good quality devices within a reasonable time. For this, an *in situ* growth method for SWNTs has been developed, based on the catalytic chemical vapor deposition (CCVD) of carbon from methane. *In situ* means that the SWNTs directly grow in their final position on the wafer. The controlled growth of 1 nm diameter SWNTs by CCVD on oxidized silicon substrates covered by a catalytic layer composed of nickel on aluminum has been demonstrated. All SWNT diameter and density measurements have been performed by AFM, which has been found to be a very useful method for non-destructive geometrical and structural characterizations of SWNTs at the nanometer scale. To the best of our knowledge, successful conductive-AFM (C-AFM) measurements have been performed on *in situ* connected SWNTs for the first time worldwide. This allows clear overviews of SWNTs and structures also on rough underlayers, which are impossible with the traditional AFM due to the nanometer size of the SWNTs.

The *in situ* growth of SWNTs has been integrated into a novel fabrication process for palladium-contacted and PMMA (polymethyl methacrylate) passivated CNTFETs, which only requires one lithography step, avoiding any misalignment problems. The major novelty of the process consists in the introduction of a sacrificial catalyst, which is evaporated on the whole wafer surface. This catalyst is composed of a well-optimized Ni/Al bilayer, which catalyzes the growth of 1 nm diameter SWNTs and simultaneously transforms itself into an insulator (aluminum oxide covered with nickel nanoclusters) during the high temperature growth process, so that there is no need to structure the catalyst after deposition. The definition of the Pd source and drain regions as well as the passivation of the channel region occur simultaneously after the SWNT growth

step by means of a single optical lithography step. The novel self-aligned fabrication process developed in this PhD thesis allows the simultaneous fabrication of approximately 1,000 transistors on one wafer (2”). Further optimization of the lithography layout could easily multiply this number. When comparing to the often practiced production of CNTFETs with external growth of SWNTs and subsequent coating or placement, this process based on the *in situ* growth method is more reliable and time-saving. It also reduces the risk of contamination of SWNTs, which leads to better device performance.

The suitability for mass fabrication of this process has been verified on more than 15,000 devices. Extended yield statistics on 700 devices have been performed, leading to the result of 41% of fully functional high on/off ratio devices within all measured devices. Optimization of the device geometry, e.g. reduction of the effective channel length, should further improve the yield drastically. Approximately 100 devices have been completely evaluated, i.e., complete sets of electrical device characteristics have been recorded and analysed to perform statistics on device performance and reliability. The devices exhibit promising electrical parameters, e.g. on-currents up to 6 mA/μm and on/off ratios up to 2.6×10^7, already at a very low drain source bias of -400 mV. Such a low-voltage low-power technology is compatible with mobile applications. Moreover, the PMMA passivation increases the life time from some weeks to several years.

The well-known hysteresis-effect in CNTFET electrical characteristics has been found to be a stable and reproducible phenomenon. It most likely originates from electron trapping and detrapping in the underlaying sacrificial oxide, i.e., the aluminum oxide. Due to their charge storing properties, CNTFETs are very suitable candidates to be used in memory applications. The operation as memory cells of the CNTFETs fabricated within this work has been tested extensively. As a result, the current ratio at the reading voltage between the logical “1” level (high current) and the logical ”0” (low current) is up to 10^6, which is, to the best of our knowledge, the highest current ratio of logical levels ever published for CNT memory cells. The “0” and “1” current levels are temporally stable indicating the possibility for non-volatile memory usage.

This PhD work clearly attests to the potential for large scale manufacturing of good quality CNTFETs for future industrial applications. Moreover, the process is also a remarkable technology platform for research on CNT electronics because a large number of devices can be realized easily and in a short time. This opens the possibility to investigate the influence of numerous fabrication parameters or environmental impacts on CNTFET electrical characteristics and reliability. Lastly, the suitability of CNTFETs used as sensors, e.g. infrared-sensors, gas-sensor or bio-sensors, could be easily investigated in the future using the CNTFET fabrication process developed within this work.

Kurzfassung

Seit der Herstellung der ersten integrierten Schaltung Ende der sechziger Jahre wurde durch geometrische Skalierung die Effizienz der Metall-Oxid-Feldeffekttransistoren (MOSFETs) kontinuierlich verbessert. Heute sind die physikalischen Grenzen dieser Skalierung erreicht: die Dicke des Gate-Oxids beträgt nur noch wenige Atomlagen, Leckströme erhöhen sich zunehmend und Kurzkanal-Effekte lassen Bauelementeigenschaften degradieren. Daher ist die Entwicklung neuer Integrationskonzepte notwendig, um die auf Silizium basierende Nanoelektronik zu erweitern oder sogar zu ersetzen. Eines dieser Konzepte besteht aus der Verwendung von Kohlenstoff-Nanoröhrchen-Feldeffekttransistoren (CNTFETs). Der aktive Teil der CNTFETs, d. h. der feldgesteuerte Bereich für den Ladungstransport zwischen Source und Drain, auch Kanal genannt, wird von einem halbleitenden einwandigen CNT (single-walled carbon nanotube, SWNT) gebildet. Das Wachstum geeigneter SWNTs repräsentiert eine der größten Herausforderungen der CNT-Technologie. Die meisten veröffentlichten Herstellungsmethoden sehen ein getrenntes Wachstum von Nanoröhrchen, entweder durch Bogenentladung oder Laserablation, vor. Diese Herstellungsprozesse sind aber nicht für die Großintegration geeignet, da sie eine externe Manipulation und Montage der SWNTs nach dem Wachstum erfordern. Da die so hergestellten CNTFETs somit nur einzeln als Prototypen verfügbar sind, sind in der Literatur auch keine Daten über die großtechnische Verwendbarkeit dieser Herstellungsprozesse hinsichtlich Prozesszeit, Kosten, Reproduzierbarkeit sowie Zuverlässigkeit der Bauelemente und Ausbeute angegeben. Produktionsansätze, die in der Zukunft die Silizium-basierte CMOS Technologie ablösen wollen, sollten nicht nur eine bessere Performanz aufweisen, es muss außerdem möglich sein, die Bauelemente in größeren Mengen zur Großintegration mit Milliarden von Transistoren auf einem Wafer herzustellen. An dieser Stelle setzt diese Arbeit an und erforscht die Möglichkeit der Großserienproduktion von CNTFETs.

Das Hauptziel dieser Doktorarbeit ist die Entwicklung eines CMOS-kompatiblen Herstellungsprozesses für CNTFETs, der eine Großserienproduktion von Bauelementen guter Qualität in einer akzeptablen Produktionszeit ermöglicht. Dafür wurde eine *in situ* Wachstumsmethode für SWNTs entwickelt, die auf der katalytisch-chemischen Gasphasenabscheidung (CCVD) von Kohlenstoff aus Methan basiert. *In situ* bedeutet, dass die SWNTs direkt auf dem für sie vorgesehenen Platz auf dem Wafer aufgewachsen werden. Der Katalysator besteht aus Nickel auf Aluminium. Durch eine Optimierung der Metallschichtdicke (bis herab zu 0,9 nm) wurde das kontrollierte Wachstum von SWNTs mit 1 nm Durchmesser demonstriert. Untersuchungen der SWNT-Durchmesser und -Dichten wurden mittels Rasterkraftmikroskopie (Atomic Force Microscopy, AFM) im Nanometer-Bereich zerstörungsfrei durchgeführt. Außerdem wurde im Rahmen dieser Arbeit weltweit erstmals die Leitfähigkeits-Rasterkraftmikroskopie (Conductive AFM, C-AFM) zur Messung von *in situ* kontaktierten SWNTs angewendet. Diese Methode erlaubt eine eindeutige Identifizierung der SWNTs und den angrenzenden Strukturen auch auf rauen Unterlagen. Dies ist mit dem konventionellen, topographischen AFM nicht möglich, wenn die Rauheit der Unterlage größer als der Durchmesser der SWNTs (ca. 1 nm) ist.

Der *in situ* Wachstumsprozess der SWNTs wurde in einem neuartigen Herstellungsverfahren für Palladium-kontaktierte und PMMA (Polymethylmethacrylat) passivierte CNTFETs integriert, das lediglich einen einzigen Lithographie-Schritt benötigt und somit Maskenjustageprobleme

vollständig vermeidet. Die wesentliche Neuerung des entwickelten Prozesses ist die Verwendung eines Opfer-Katalysators. Dieser besteht aus einer Ni/Al-Doppelschicht, welche ganzflächig aufgebracht und im Gegensatz zu anderen Verfahren anschließend nicht strukturiert wird. Daher findet das Wachstum der SWNTs ganzflächig statt. Durch präzise Optimierung der Metalldicke katalysiert die Ni/Al-Doppelschicht das Wachstum von SWNTs mit 1 nm Durchmesser und wird gleichzeitig während des Hochtemperaturwachstumsprozesses in einen Isolator (mit Ni-Nanopartikeln bedecktes Aluminiumoxid) umgewandelt. Dadurch werden Kurzschlüsse zwischen den nachfolgend strukturierten Source- und Drain-Elektroden vermieden. Die Strukturierung der Palladium-Source- und Drain-Elektroden, sowie die Passivierung der Bauelemente werden zeitgleich mittels eines einzigen Lithographie-Schrittes durchgeführt. Der in dieser Arbeit entwickelte neuartige selbstjustierte Herstellungsprozess erlaubt die parallele Herstellung von etwa 1.000 Transistoren auf einem Wafer (2”). Eine Optimierung des Layouts könnte diese Zahl vervielfachen. Verglichen mit der oft benutzten Herstellung von CNTFETs mittels externem SWNT-Wachstum und anschließender manueller Manipulation, ist der hier entwickelte Prozess zuverlässiger und schneller. Außerdem reduziert er das Risiko der Kontamination der SWNTs, und verbessert so die elektrische Performanz der Bauelemente.

Die Brauchbarkeit des Prozesses für die Massenfertigung wurde mit der Herstellung von mehr als 15.000 CNTFETs demonstriert. Ausführliche Statistiken über die Ausbeute wurden auf Basis von 700 Bauelementen erhoben. Der Anteil voll funktionsfähiger CNTFETs mit hohem On/Off-Stromverhältnis beträgt 41%. Eine zukünftige Optimierung der Geometrie der Teststrukturen, beispielsweise durch Verkürzung der Kanallänge, soll die Ausbeute noch weiter verbessern. Annähernd 100 CNTFETs wurden im Rahmen der Arbeit vollständig charakterisiert, indem eine Vielzahl elektrischer Eigenschaften gemessen und analysiert wurde, um statistisch belastbare Aussagen über Bauelementperformanz und -zuverlässigkeit zu erhalten. Schon bei einer sehr niedrigen Drain-Source-Spannung von -400 mV zeigen die Bauelemente mit einem On/Off-Verhältnis von bis zu 2.6×10^7 und einem On-Strom von bis zu 6 mA/μm sehr gute Eigenschaften, so dass hierdurch die entwickelte Technologie für mobile low-power Anwendungen nutzbar ist. Die zusätzliche Passivierung der CNTFETs mit PMMA erhöht deren Lebensdauer von wenigen Wochen auf mehrere Jahre.

Durch weitere Untersuchungen konnte der aus der Literatur bekannte Hysterese-Effekt in der Transferkennline eines CNTFET als konstantes und reproduzierbares Phänomen bestätigt werden. Als wahrscheinlichste Ursache der Hysterese erwies sich hierbei, dass Elektronen im Aluminium Oxid (Teil des Opfer-Katalysators) eingefangen und wieder freigesetzt werden. Aufgrund des Ladungseinfangs erscheinen CNTFETs für Speicheranwendungen sehr geeignet zu sein. Die Funktionsfähigkeit der CNTFETs als Speicherzellen wurde ebenfalls in dieser Arbeit untersucht. Das Verhältnis zwischen logischer “0” und “1” beträgt bis zu 10^6. Dies ist, soweit bekannt, das höchste, je veröffentlichte Stromverhältnis zwischen logischen Zuständen für CNT Speicherzellen. Die “0” und “1” Zustände sind zeitlich stabil, sodass eine Nutzung der Bauelemente als nichtflüchtige Speicher möglich erscheint.

Die Ergebnisse dieser Arbeit zeigen das eindeutige Potential der CNT-Technologie für eine Großserienherstellung von hochwertigen Bauelementen für zukünftige industrielle Anwendungen. Mit dem hier vorgestellten Prozess kann eine große Zahl an Bauelementen auf einfache Weise hergestellt werden. Hiermit steht nun eine Technologie-Plattform für die zukünftige CNT-Forschung zur Verfügung, die es gestattet, sowohl den Einfluss zahlreicher Herstellungs- als auch Umweltparameter auf die elektrischen Eigenschaften der CNTFETs zu untersuchen. Schließlich können CNTFETs auch in anderen Anwendungen mittels des in dieser Arbeit entwickelten Her-

stellungsverfahrens eingesetzt und untersucht werden. Als Beispiele für weitere Forschungsgebiete sind die Untersuchung der CNTFETs als Infrarot-Detektoren, Gas- oder Bio-Sensoren zu nennen.

Contents

1 Introduction 1

2 CNT basics and theoretical considerations 5

2.1 Discovery of carbon nanotubes . . . 7

2.2 Introduction to single-walled carbon nanotubes . . . 8
- 2.2.1 Diameter . . . 8
- 2.2.2 Crystalline structure . . . 9
- 2.2.3 Metallicity . . . 12
- 2.2.4 Band structure . . . 14
- 2.2.5 Electronic transport . . . 24
- 2.2.6 Synthesis methods . . . 25

2.3 Carbon Nanotube Field-Effect Transistor (CNTFETs) . . . 26
- 2.3.1 Metal-semiconductor contact . . . 26
- 2.3.2 CNTFET operation . . . 27

2.4 Carbon nanotube applications . . . 36

2.5 Conclusions and motivation for this PhD work . . . 38

3 Development of *in situ* growth method for SWNTs and associated characterization technique 39

3.1 *In situ* growth of SWNTs by means of catalytic chemical vapor deposition (CCVD) . . . 41
- 3.1.1 Setup description . . . 41
- 3.1.2 Parameters of SWNT growth . . . 44

3.2 Characterization of *in situ* grown SWNTs by atomic force microscopy (AFM) . . . 47
- 3.2.1 Principle of AFM and presentation of AFM Dimension 3100 . . . 47
- 3.2.2 Basic AFM measurements on catalyst and SWNTs . . . 50
- 3.2.3 AFM optimization of catalyst thickness to control SWNT diameter . . . 54
- 3.2.4 Limitations of AFM . . . 61

3.3 Conductive atomic force microscopy (C-AFM) on SWNTs . . . 63
- 3.3.1 Principle of C-AFM . . . 63
- 3.3.2 C-AFM measurements on SWNTs . . . 64

3.4 Conclusion . . . 67

4 Self-aligned process for large scale fabrication of CNTFETs 69

4.1 Preparatory work . . . 71
4.1.1 Mask for optical lithography . . . 71
4.1.2 Semiconductor parameter analyzers . . . 73

4.2 First attempt on CNTFET fabrication using catalytic areas as source/drain electrodes . . . 73

4.3 Development of a novel fabrication process based on "sacrificial catalyst" for high on/off ratio CNTFETs . . . 77
4.3.1 Introduction to "sacrificial catalyst" and C-AFM measurements . . . 77
4.3.2 CNTFET fabrication process and associated C-AFM characterization method . . . 79
4.3.3 Macroscopical electrical measurements of CNTFETs . . . 84
4.3.4 Analysis and experiments on hysteresis . . . 93

4.4 PMMA passivation of CNTFETs . . . 100
4.4.1 Motivation and concept to improve long term stability . . . 100
4.4.2 PMMA self aligned contacting and passivation of CNTFETs . . . 100
4.4.3 Measurements and evaluation of PMMA-passivated CNTFETs . . . 102

4.5 Conclusion . . . 105

5 Analysis of large-scale production of CNTFETs and applications for future industrial use 107

5.1 Statistical evaluation of CNTFET fabrication process. . . . 109
5.1.1 Definitions and framework of statistical evaluation. . . . 109
5.1.2 Process yield, good quality devices percentage and device type distribution. . . . 111
5.1.3 Influence of device geometry on process yield and device type distribution. . . . 112
5.1.4 Attempts to improve yield by piranha cleaning . . . 114

5.2 Discussion on devices with small on/off ratios or metallic SWNT S/D links . . . 115

5.3 Analysis of CNTFET electrical parameters based on a large number of devices. . . . 117
5.3.1 Preliminary remarks on nominal/effective channel lengths and widths . . . 117
5.3.2 Statistics and discussion on electrical parameters . . . 119
5.3.3 Performance evaluation - ITRS benchmark . . . 126
5.3.4 Performance evaluation - Comparison with other CNTFETs . . . 129

5.4 Application of CNTFETs as memory cells . . . 131

5.5 Conclusion . . . 134

6 Conclusions and future prospects 135

6.1 Conclusions . . . 137

6.2 Future prospects . . . 138

Appendix 141

List of publications and conference contributions 143

Bibliography 146

Curriculum vitae 155

List of abbreviations

Al	Aluminum
Al_2O_3/ Al_xO_y	Aluminum oxides
AFM	Atomic Force Microscopy or Microscope
C_{60}	Buckminsterfullerene
C-AFM	Conductive Atomic Force Microscopy or Microscope
CMOS	Complementary Metal Oxide Semiconductor
CNT	Carbon Nanotube
CNTFET	Carbon Nanotube Field-Effect Transistor
CH_4	Methane
CVD	Chemical Vapor Deposition
CCVD	Catalytic Chemical Vapor Deposition
DWNT	Double-Walled Carbon Nanotube
EOT	Equivalent Oxide Thickness
FET	Field-Effect Transistor
H_2	Hydrogen molecule
HF	Hydrofluoric Acid
HRTEM	High Resolution Transmission Electron Microscope
H_2O_2	Hydrigen peroxide
H_2SO_4	Sulfuric acid
ISTN	Institute for Semiconductor Technology and Nanoelectronics (Institut für Halbleitertechnik und Nanoelektronik)
ITRS	International Technology Roadmap for Semiconductors
MOS	Metal Oxide Semiconductor
MOS-CNTFETs	Metal Oxide Semiconductor Carbon Nanotube Field-Effect Transistor
MOSFET	Metal Oxide Semiconductor Field-Effect Transistor
MWNT	Multi-Walled Carbon Nanotube
N_2	Nitrogen molecule
Ni	Nickel
NMP	N-Methyl-2-pyrrolidone
OC-CNTFET	Ohmic Contact Carbon Nanotube Field-Effect Transistor
Pd	Palladium
PMMA	Polymethyl Methacrylate
SB	Schottky Barrier
SB-CNTFETs	Schottky Barrier Carbon Nanotube Field-Effect Transistor
SBH	Schottky Barrier Height
S/D	Source/Drain

continued on next page

SEM	Scanning Electron Microscope
SiO_2	Silicon Dioxide
SWNT	Single-Walled Carbon Nanotube
s-SWNT	Semiconducting Single-Walled Carbon Nanotube
m-SWNT	Metallic Single-Walled Carbon Nanotube

List of symbols

a	Length of graphene lattice unit vectors ($=\sqrt{3}a_{C-C}$)
$(\overrightarrow{a_1}, \overrightarrow{a_1})$	Unit vectors of graphene lattice
a_{C-C}	Carbon-carbon bond length (1.44 $\AA$)
$(\overrightarrow{b_1}, \overrightarrow{b_1})$	Unit vectors of reciprocal space of graphene lattice
Acc	Electron/hole acceleration in electric field
$\overrightarrow{C}$	Chiral vector
χ_{SWNT}	SWNT electron affinity
d_{SWNT}	SWNT diameter
d_q	Quartz thickness
d_l	Thickness of evaporated layer
E	Energy state
E_F	Fermi level
E_g	Band Gap
$E(\overrightarrow{k})$	Eigenfunctions at wave vector $\overrightarrow{k}$
f	Quartz eigenfrequency
Δf	Quartz frequency shift after evaporation
$f_{Fermi-Dirac}(E)$	Fermi-Dirac statistics
G_0	Conductance quantum (= 2 q^2/h = 77.5 μS)
Γ	Center of the hexagonal unit-cell of graphene lattice
H	Hamiltonian
h	Planck constant (6.626 10^{-34} m^2 kg / s)
I_{ds}	Drain-Source Current
I_{off}	Off-Current
I_{on}	On-Current
k	Boltzmann constant
$\overrightarrow{k}$	Wave vector
K_{1to6}	Apexes of the hexagonal unit-cell of graphene lattice
L_{nom}	Nominal device channel length
m_q	Mass of quartz
Δm_q	Mass of evaporated layer
M_{1to6}	Middles of the sides of the hexagonal unit-cell of graphene lattice
(n,m)	SWNT integers
$\mathscr{P}$	Projection of $\overrightarrow{b}_1$ on $\overrightarrow{a}_1$
$\phi_{B,n}$	Potential barrier for electrons at the semiconductor/metal contact
$\phi_{B,p}$	Potential barrier for holes at the semiconductor/metal contact

continued on next page

ϕ_M	Metal work function
ϕ_{SWNT}	SWNT work function
$\psi(\overrightarrow{k})$	Eigenvalues at wave vector $\overrightarrow{k}$
q	Elementary charge, i.e., magnitude of the charge of an electron (1.602 10^{-19} Coulombs)
ρ_q	Density of quartz
ρ_l	Density of evaporated layer
R_{on}	On-resistance
T	Temperature
Tu	Tunneling conduction
Th	Thermionic conduction
V_g	Gate Voltage
V_{gs}	Gate-Source Voltage
V_{ds}	Drain-Source Voltage
$V_{ds,sat}$	Drain-Source Voltage indicating the beginning of the device saturation range
V_{th}	Threshold voltage
$V_{th,f}$	Threshold voltage of the forward sweep
$V_{th,b}$	Threshold voltage of the backward sweep
W_{nom}	Nominal device channel width
$\mathbb{Z}$	Set of integers
$\mathbb{Z}^*$	Set of non-zero integers

List of Equations

(2.1) Chiral vector . . . 11
(2.2) SWNT circumference (length of chiral vector) . . . 11
(2.3) SWNT diameter (based on (n,m) integers) . . . 11
(2.4) Fermi-Dirac statistics . . . 15
(2.5) Definition of reciprocal space . . . 15
(2.6) Schrödinger's equation (independent of the time) . . . 15
(2.7) Reciprocal space definition in the two dimensional case . . . 17
(2.8) Electronic band structure of graphene . . . 18
(2.9) Quantization condition of the wave in a periodical potential . . . 19
(2.10) Quantization of k . . . 19
(2.11) Condition of quantization for armchair SWNTs . . . 20
(2.12) Calculation of the distance ΓM in reciprocal space of graphene . . . 20
(2.13) Condition of quantization for zigzag SWNTs . . . 22
(2.14) Calculation of the distance ΓK_6 in reciprocal space of graphene . . . 22
(2.15) Calculation of the distance $M'K_1$ in reciprocal space of graphene . . . 22
(2.16) SWNT band gap versus diameter . . . 24
(2.17) SWNT electron affinity . . . 29
(2.18) Schottky barrier heights for electrons . . . 29
(2.19) Schottky barrier heights for holes . . . 29
(3.1) Relation between quartz crystal mass and frequency . . . 44
(3.2) Calculation of evaporated metal thickness . . . 44
(4.1) CVD of carbon from methane . . . 77
(4.2) Definition of hysteresis . . . 88
(4.3) Shift of backward sweep due to electron injection . . . 99
(5.1) Equivalent gate capacitance for SiO_2/Al_2O_3 double gate oxide . . . 128
(5.2) SiO_2 underlayer thickness for EOT of 5 nm . . . 128

List of Figures

2.1 SEM micrograph of CNTs, probably the first published image of a CNT. Famous HRTEM micrograph of MWNTs published by Iijima in 1991. . . . 7
2.2 Simultaneous discovery of SWNTs from Iijima et al. and Bethune et al. . . . 8
2.3 Different forms of carbon with an hexagonal lattice. . . . 9
2.4 Occupation of the atomic orbitals of carbon and sp^2 hybridization. . . . 10
2.5 σ and π bonding of carbon by graphite, graphene and carbon nanotubes. . . . 11
2.6 Example of armchair/zigzag SWNT. . . . 12
2.7 Representation of all SWNTs with a diameter between 0.950 and 1.059 nm. . . . 14
2.8 Electronic band structure of silicon along the lines of symmetry within the first Brillouin zone. . . . 16
2.9 Schematic of graphene in the real and reciprocal spaces. . . . 17
2.10 Graphene band structure 18
2.11 Left: Representation of an infinite SWNT in the plane and its quantized wave vectors. Center: Illustration of supplementary SWNT quantization on graphene 2D band structure. Right: Example of SWNT band structure. . . . 20
2.12 Left: Allowed wave vectors lines of (6,6) SWNT. Center: View of graphene band structure "from the MK perspective". Right: Electronic band structure of (6,6) SWNT. . . . 21
2.13 (a): Left: allowed wave vectors of (12,0) SWNT. Middle: view of graphene band structure "as seen from line 1". Right: Band structure of (12,0) SWNT. (b): Left: allowed wave vectors of (13,0) SWNT. Right: Band structure of (13,0) SWNT. . . . 21
2.14 Left: allowed wave vectors of (6,3) m-SWNT. Right: allowed wave vectors of (7,3) s-SWNT. 23
2.15 STM scan and I-V measurement results from Odom et al. . . . 24
2.16 Contact formation of a metal/SWNT/metal structure. Metal work function: 4.7 eV. The structure corresponds to a mid gap CNTFET. . . . 30
2.17 Conduction mechanism in mid gap CNTFET. . . . 31
2.18 Contact formation of a Pd/SWNT/Pd structure. . . . 32
2.19 Conduction mechanism in Pd contacted CNTFET. . . . 33
2.20 Contact formation of an Al/SWNT/Al structure. . . . 34
2.21 Conduction mechanisms in Al contacted CNTFET. . . . 35
2.22 Transfer characteristics of CNTFETs used in different sensor applications. . . . 37
3.1 Photograph of CVD setup at ISTN. . . . 42
3.2 SEM micrograph of CNTs grown from cluster. Magnification 50,000. . . . 43
3.3 Photograph of electron beam evaporation setup at ISTN. . . . 43
3.4 SEM pictures of CNTs grown by CVD. Magnification: 10,000 X. . . . 46
3.5 Top: schematic of AFM, Bottom left: SEM micrograph of a silicon cantilever substrate from Budget Sensors. Bottom right: Interaction force versus distance between tip and sample. . . . 48

3.6 Left: bottom view of cantilever holder from AFM Dimension 3100. Right: Photo of AFM Dimension 3100 (Digital Instruments/Veeco). 49
3.8 Example of AFM scan (amplitude) of CNTs extending from structured catalytic area and lying on smooth SiO_2. 51
3.9 Left: SEM overview of structured catalyst on SiO_2. Middle and right: Comparison of SEM micrograph with AFM scan (amplitude) showing exactly the same place on the wafer. . . . 52
3.10 Three examples of AFM scans (amplitude) illustrating CNTs growth from Ni-clusters. . . . 52
3.12 AFM scans (amplitude) showing the difference in cluster formation and in density and size of nanotubes without (left) and with (right) oxygen plasma. 54
3.13 Left: AFM scan (height) on evaporated catalyst (Al/Ni, nominal thickness: 15 nm) before growth. Right: associated measurement of stepheight with AFM function “stepheight”. . . 55
3.14 Distribution of diameter (measured by AFM) of CNTs grown on 10 nm Ni/10 nm Al. 56
3.15 Influence of Ni thickness on SWNT diameter for a constant Al nominal thickness (10 nm). Left column: AFM scans (height). Right column: cross sections along respective white lines. 57
3.16 Influence of Al thickness on SWNT diameter for a constant Ni nominal thickness ($\sim$ 1 nm). Left column: AFM scans (height). Right column: cross sections along corresponding white lines. 58
3.17 Diameter uniformity of SWNTs grown from the same catalytic structure. 59
3.21 Schematic of C-AFM measurement setup. 63
3.22 (a) to (c): C-AFM scans (current) where bright areas show catalytic areas (Al/Ni) and connected CNTs. (d): Example of I/V sweep measured on SWNT. 65
3.23 Simultaneously measured C-AFM topographical and electrical information illustrating the broadening effect. 66
4.1 (a): Layout of the whole mask used for lithography step. (b) to (d): Details of the mask layout representing CNTFETs with different geometries. 72
4.2 Schematic of CNTFET in which catalytic areas are directly used as S/D electrodes. 73
4.4 (a): Schematic of CNTFET where Pd S/D electrodes are aligned on catalytic areas. (b): Example of AFM scan (height) of a CNTFET fabricated by aligning Pd electrodes on catalytic areas showing the difficulty of this process and the misalignment problem. 75
4.6 Schematic of test structure for AFM sacrificial catalyst investigation 77
4.7 Comparison of C-AFM height and current scans on structured sacrificial catalyst. 78
4.8 Steps of the self-aligned fabrication process for Pd-connected CNTFETS. 80
4.9 Schematic of intermediate steps and final structure of the fabrication process for CNTFET reported in this chapter. 81
4.10 SEM micrograph of the undercut formed by the PMMA under the photoresist. 82
4.11 Comparison of tapping-mode and conductive mode AFM measurements on sacrificial catalyst. 83
4.12 Utilization of C-AFM scans (current images) to evaluate SWNT density. 84
4.13 Detection of CNT linking S/D with C-AFM. Link column: no CNT link, right column: with CNT links. 85
4.14 Schematic of electrical measurement setup for CNTFET characterization. 86
4.15 Example of transfer characteristics obtained on a CNTFET fabricated with the self-aligned fabrication process reported in this section. SiO_2 thickness: 50 nm. 87
4.16 Four examples of CNTFET transfer characteristics measured on three different wafers, all with a SiO_2 thickness of 50 nm. 89
4.17 Example of output characteristics obtained on device with s-SWNT as channel. The dashed lines are linear approximations of the sweeps. 90
4.18 Results from Hoenlein et al. Left: ideal output characteristics. Right: degradation of output characteristics with source and drain contact resistances of 50 kΩ. 90

4.22 Analysis of hysteresis and threshold voltages evolution with increased symmetrical gate voltage cycling ranges. 96
4.24 Measurement of transfer characteristics with different unsymmetrical gate voltage cycling ranges. 98
4.25 Transfer characteristics of CNTFET starting with -1 V and ending with 0.74, 0.8 and 0.84 V. Only the last measurement shows hysteresis. 99
4.28 Reproducibility of transfer characteristics of devices after about one year. 104
5.1 Process yield, all wafers together. 111
5.2 Distribution of device type within functional devices. 111
5.3 Distributions of good quality devices within all devices. 112
5.4 Dependency of non-working device percentage with nominal device channel width. Dependency of device type distribution with nominal device channel width. 113
5.5 Evolution of the process yield and the devices distribution with increasing S/D spacing. . . 113
5.7 Statistics on CNTFETs fabrication process with piranha cleaning. All S/D spacings and widths together. 115
5.10 Experiment to demonstrate the possibility that devices with small on/off ratio have two parallel SWNTs as channel: one metallic and one semiconducting. 117
5.11 Schematic of CNTFET indicating nominal channel length and width, as well as effective channel width and shorter and longer possible effective channel lengths. 118
5.12 Distribution and average value of the on-current for different silicon dioxide thicknesses. . 120
5.13 Influence of S/D electrodes width on on-current. Total devices: 37. SiO_2 thickness: 37-40 nm. S/D spacing: 2 to 4 μm, considered here as equivalent. 121
5.14 Distribution and average value of off-current for different silicon dioxide thicknesses. The x axis has a logarithmic scale. 122
5.15 Distribution and average value of the on/off ratio for different SiO_2 thicknesses. The x axis has a logarithmic scale. 122
5.16 Distribution and average value of the slope for different SiO_2 thicknesses. 123
5.17 Mean slope versus SiO_2 thickness, from Fig. 5.16. 123
5.18 Distribution and mean value of threshold voltages for different SiO_2 thicknesses. 124
5.19 Distribution and average value of the hysteresis for different SiO_2 thicknesses. 124
5.20 On/off ratio versus hysteresis for devices with I_{on} >5 10^7. 125
5.21 Hysteresis versus SiO_2 thickness for devices with on/off ratio > 10^3. All S/D dimensions together. Total devices: 90. 126
5.22 Transfer characteristics of CNFTET: development of hysteresis width (i.e., memory window) with increasing gate voltage cycling range, basics of memory operation. Oxide thickness: 40 nm. 131
5.23 Cycling of CNTFET memory cell. Applied gate voltage and measured drain-source current plotted versus time. 132
5.24 Reproducibility of drain voltage levels for different applied gate voltage cycles. 133
6.1 Illustration of proposed CNTFET-sensor for virus detection. The semiconducting SWNT is functionalized with a suitable receptor to allow selective bonding of virus. 139

List of Tables

2.1 Metallicity of SWNTs according to their integers (n,m). 13
2.2 Calculated diameters of all SWNTs with a diameter between 0.950 and 1.059 nm. 14
2.3 Parameters of mid gap CNTFET 29
2.4 Parameters of Pd contacted CNTFET 32
2.5 Parameters of Al contacted CNTFET 34
3.1 Comparison of nominal and effective Al/Ni thicknesses, influence on SWNT diameter. . . . 56
3.2 Diameters of SWNTs shown on Fig. 3.17 59
4.1 Influence of catalyst thickness on the quantity of working CNTFETs. 86
5.1 Classification of CNTFETs according to their transfer characteristics. 110
5.2 Process yield for each of the eight wafers. 111
5.3 Distributions of device type, for each of the eight wafers. 111
5.4 Distributions of good quality devices within all devices, for each of the eight wafers. 112
5.5 Effective channel lengths according to nominal device length and width. 119
5.6 Extract of the ITRS 2007 127
6.1 Performances of CNTFETs fabricated within this PhD, with an SiO_2 thickness of approximately 30 nm. 138

Chapter 1

Introduction

Since the first integrated circuits in the late 1960's, a constant improvement of their performances could be reached by scaling down the metal oxide semiconductor field-effect transistors (MOSFETs). The down scaling is predicted by the well-known Moore's law, which enunciates that the number of devices on a chip should double every 18 months. At the same time, the speed should increase whereas the cost should decrease. However, downscaling of MOS transistors has reached its physical limits: the gate oxide is only composed of a few atomic layers, leakage currents are increasing and the short channel effects degrade device properties. These are the reasons why new integration concepts need to be developed to replace silicon based nanoelectronics.

Carbon nanotubes are hollow cylinders of hexagonal arranged carbon atoms. Single-walled carbon nanotubes (SWNTs), which are composed of a single cylinder, can be metallic or semiconducting depending on their structure. Semiconducting SWNTs can act as the channel in a new generation of FETs, the so-called carbon nanotube field-effect transistors (CNTFETs). CNTFETs are acknowledged as a possible replacement of traditional MOSFETs in the complementary metal oxide semiconductor (CMOS) technology to develop advanced logic circuits, so that Moore's law can still be followed in the future. CNTFETs belong to the so-called molecular electronics, which also include all devices based on silicon nanowires or other kinds of nanotubes (e.g. boron nitride). The approach of molecular electronics differs from the conventional electronics manufacture. Indeed, the conventional technology is based on the top-down approach, i.e., macroscopic silicon wafers are structured to obtain billions of tiny devices, which are constantly miniaturized year after year. Molecular electronics uses the bottom-up assembly principles, i.e., tiny molecules are taken as basis of the structure to build the device.

However, a candidate for replacing the MOSFET should not only have better performances but it should also be possible to produce it in large quantities to allow integration on a very large scale, i.e., billions of transistors on one wafer. Most of the CNTFETs have been described as being fabricated by manually placing the nanotubes on the wafer, either only by spin coating or by nanomanipulation, for instance via atomic force microscopy (AFM). Nanomanipulation is probably incompatible with large scale fabrication.

The primary aim of this PhD work is the development of a CMOS compatible fabrication process for CNTFETs which allows large scale production of devices within a reasonable time. For this, an *in situ* growth method for single-walled carbon nanotubes (SWNTs) is chosen, based on chemical vapor deposition (CVD) of carbon from methane. The quality of the process should be tested in terms of device performance but also in terms of yield. In fact, many reports are available on advanced nanotube devices with high performances, but only very few descriptions can be found on large scale integration of carbon nanotubes enhanced with statistics on yield and device reproducibility. The second aim of this work is the evaluation of CNTFETs as eventual replacement for MOSFETs, as well as the investigation of other applications of CNTFETs to be used in integrated circuits.

This dissertation starts with an introduction on carbon nanotube basics (chapter 2): their discovery, the structure of SWNTs, CNT synthesis, applications and finally, the description of CNTFET operation. This part is followed by three chapters on experiments and results. The first one, chapter 3, deals with the *in situ* growth method of SWNTs developed within this PhD work as well as its associated characterization method based on atomic force microscopy. Chapter 4 describes the development of a novel self aligned fabrication process for palladium contacted and PMMA passivated CNTFETs based on the *in situ* growth of SWNTs. Chapter 5 provides a detailed statistical evaluation of this process in view of several future applications of CNTFETs in

industrial practice. Chapter 6 summarizes the results presented in this dissertation and gives an outlook of the future work which can be performed on the basis of this PhD to further improve the performance and understanding of SWNTs and SWNT *in situ* growth.

Chapter 2

CNT basics and theoretical considerations

Carbon nanotubes (CNTs) are hollow cylinders made exclusively of carbon atoms. Since their length, in the micrometer range, is much larger than their diameter (a few nanometers), CNTs can be considered as *one-dimensional* molecules. This chapter starts with the discovery of CNTs (section 2.1). Then, as this PhD work focuses only on single-walled carbon nanotubes (SWNTs), an introduction on SWNTs is given, summarizing their physical and electronic structures, their electrical properties and their synthesis methods (section 2.2). Subsequently, the electrical operation of carbon nanotube field-effect transistors (CNTFETs) is described, based on several theoretical studies reported in literature as well as on the most relevant experimental results published within the scientific community on these novel devices (section 2.3). The next section (section 2.4) gives a short overview on the numerous possibilities of integrating carbon nanotubes in electronic devices. Finally, a conclusion of this chapter is given, as well as the motivation for this PhD work.

2.1 Discovery of carbon nanotubes

In scientific literature, the experimental discovery of carbon nanotubes is usually attributed to the Japanese researcher Sumio Iijima from NEC in 1991 [1]. However, the first report on carbon nanotubes dates back to 1952 and was published in the Soviet Union (see Fig. 2.1a) [2]. As it was written in Russian, the report remained unknown for the rest of the world.

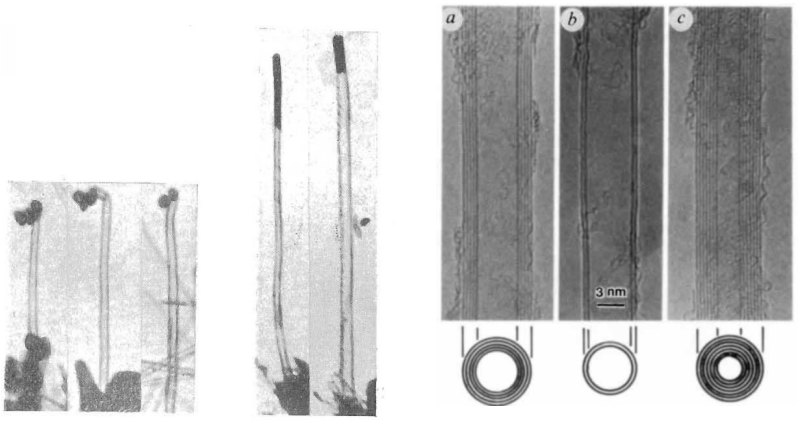

(a) (b)

Figure 2.1: (a) SEM micrograph of CNTs taken from [2]. Probably the first published image of a CNT. Magnification 20000. (b) Famous HRTEM micrograph of MWNTs published by Iijima in 1991 [1].

Carbon nanotubes were probably produced even before 1952 but their unique one-dimensional structure combined with a size in the nanometer range could only be observed under a high resolution transmission electron microscope (HRTEM). In 1971, S. Iijima developed one of the world's first HRTEM at the Arizona State University in USA and was able to see the atomic structure of metal [3]. Ten years later, by working on different carbon materials, he saw onion-shaped carbon structures in carbon soot obtained from an arc discharge without giving more attention to them. In 1985 Kroto et al. reported on these new structures [4]. The so-called buckminsterfullerene are stable football-like clusters of 60 carbon atoms, with 12 pentagons and 20 hexagons (see Fig. 2.3 in the next section). Harold W. Kroto, Richard E. Smalley, and Robert F. Curl received the Nobel prize in chemistry in 1996 for the discovery of the fullerenes.

After the publication by Kroto et al., the interest in carbon nanostructures increased and S. Iijima started working again on them at NEC in Japan. He was trying to obtain pictures of the C_{60} nanomolecules with the HRTEM when he observed in 1991, for the first time the shell structures of multi-walled carbon nanotubes (MWNT) (see Fig. 2.1b) [1].

In Iijima's pictures, several concentrically arranged shells could be recognized so that the discovery of carbon nanotubes with only one shell, the so-called single-walled carbon nanotubes (SWNTs), was just a question of time. Physical and electronic properties of SWNTs has already been calculated by three separated groups, two in USA [5, 6] and one in Japan [7] even before SWNTs had been observed for the first time. Two years later, simultaneously with IBM researchers (see Fig. 2.2b) [8], Iijima and Ichihashi published their observations of SWNTs (see Fig. 2.2a) [9]. From this moment on, the interest and the enthusiasm for carbon nanotubes in all scientific areas such as electronics, sensor technology, material science, chemistry and biology, began and is nowadays still growing.

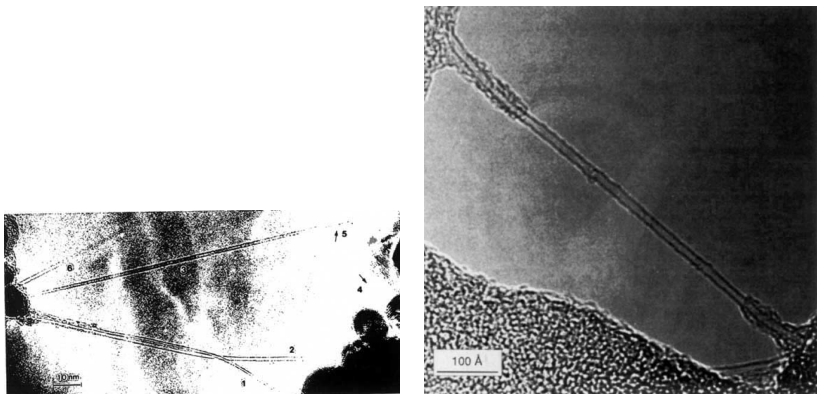

(a) (b)

Figure 2.2: Simultaneous discovery of SWNTs from (a) Iijima et al. [9] and (b) Bethune et al. [8]

2.2 Introduction to single-walled carbon nanotubes

SWNTs, carbon nanotubes with only one shell, excite considerable interest in the scientific community because of their particular characteristics. Similar to MWNTs, they are very robust due to the C-C bond, one of the strongest bonds in nature. However, they are even more one-dimensional as their diameter is only approximately 1 nm, whereas their length, typically in the μm to mm range, can reach several cm [10]!

2.2.1 Diameter

The question of the thinnest stable SWNT was clarified in the theoretical calculations of Sawada and Hamada in 1992 [11]. They predicted that the minimum diameter for an energetic stable SWNT is about 0.4 nm. The experimental observation of the smallest SWNT is a disputed topic, because SWNTs with a diameter of 0.4 nm are the ultimate one-dimensional molecule. In 2000, Qin et al. demonstrated a HRTEM micrograph of a MWNT whose innermost shell measures 0.4 nm [12]. At the same time, Wang et al. published a HRTEM micrograph of porous zeolite single crystals which contain a SWNT with a visible diameter of 0.42 nm in their

center [13]. The simple measurement method which both groups used, namely a direct geometrical measurement on a HRTEM micrograph, is questionable because they could not exactly identify the *chirality* of their nanotubes (see subsection 2.2.2) to confirm the diameter. Maybe these nanotubes were much wider than claimed. Very recently, DWNTs (double-walled carbon nanotubes) with innermost shells of 0.3 - 0.4 nm could be unambiguously observed experimentally by HRTEM [14]. To this day, no one has been able to observe an individual SWNT (i.e., not encapsulated into another structure) with a diameter of 0.4 nm. Typical diameters of SWNTs grown by different methods which can be found in literature range between 0.7 nm and 3 nm. SWNTs which are energetically the most stable, have a diameter of 1.4 nm. Nanotubes with a diameter greater than 2.5 nm are most likely DWNTs rather than SWNTs for energetic reasons.

2.2.2 Crystalline structure

A crystal is a material in which atoms are placed in a highly ordered structure. The crystalline structure of SWNTs has to be imagined as the hexagonal honeycomb lattice of graphene (i.e., a single layer of graphite) which is rolled up (see Fig. 2.3). This lattice is only composed of carbon

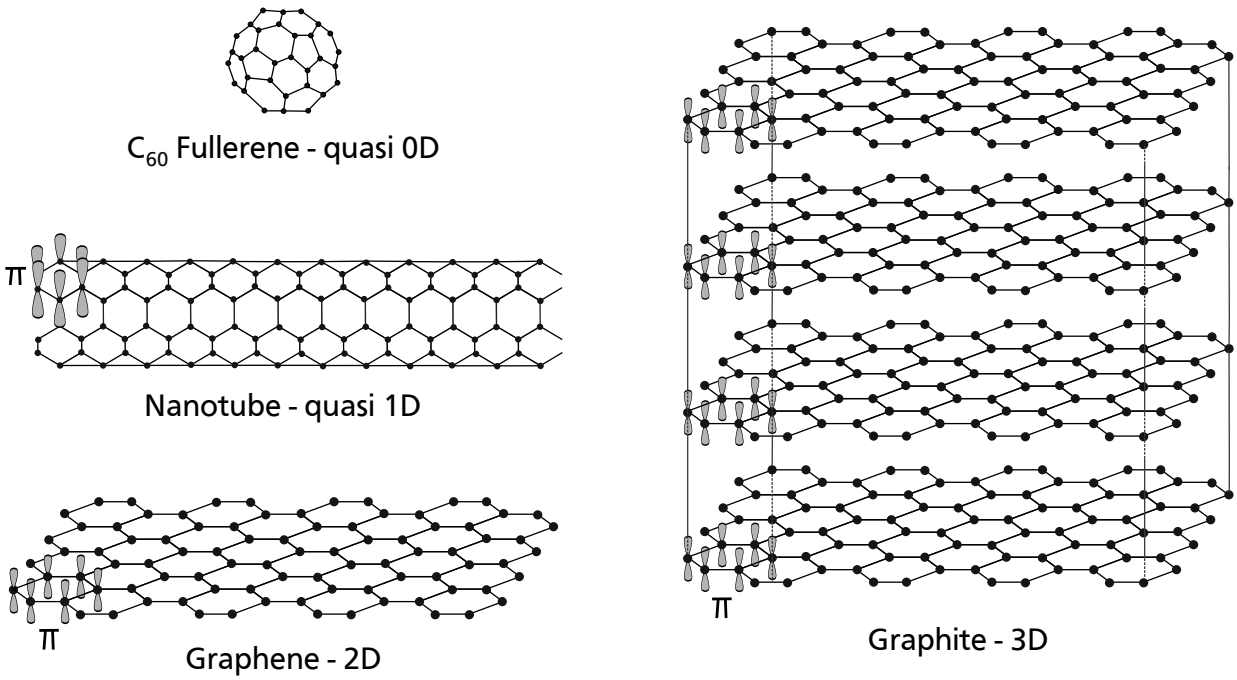

Figure 2.3: Different forms of carbon with an hexagonal lattice. All points represent a carbon atom. Fullerenes can be considered as quasi zero dimensional structures due to their comparatively tiny size: The C_{60} molecule represented here has a diameter of only 0.7 nm [4].

atoms. To understand carbon bonding in SWNT lattice, the electronic structure of carbon atoms should first be described.

In free atoms, the energy of electrons can only take discrete values, called *energy levels or states*. Quantum mechanics treats electrons as waves and particles. It describes the energy states which are *allowable* to an electron in an atom, and the *probability* for an electron to occupy one given energy state when no extern energy is applied to the atom. *Atomic orbitals* represent the probability distribution of an electron in an atom or molecule.

A carbon atom exhibits six electrons, which can occupy the atomic orbitals with the lowest energies: 1s, 2s and 2p. Two of the six electrons are core electrons (1s orbital). In the lowest energy state of carbon atoms, two valence electrons occupy the 2s orbital and the two other valence electrons occupy the 2p orbital (see Fig. 2.4 top left). However, the energy of the 2p

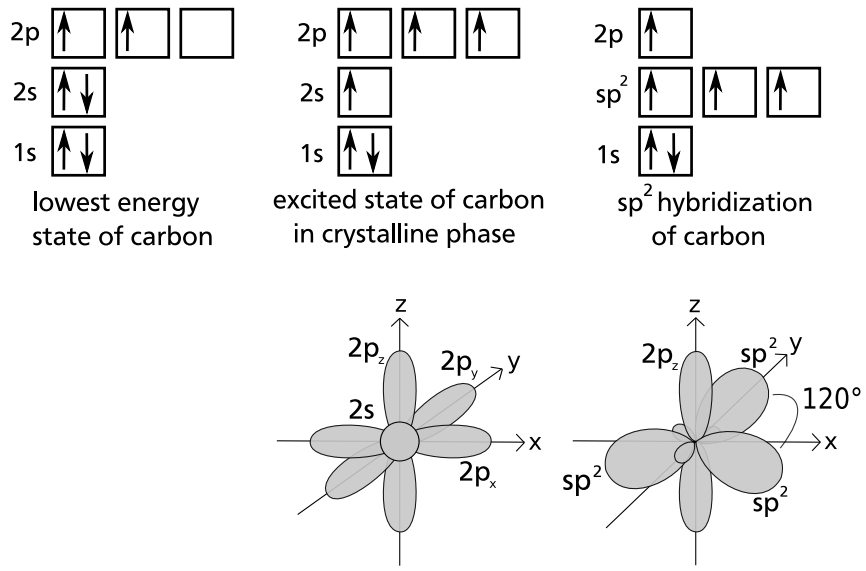

Figure 2.4: Occupation of the atomic orbitals of carbon and sp^2 hybridization.

and 2s orbitals are almost identical. In the crystalline phase, carbon atoms form an excited state by promoting one of the 2s electrons into an empty 2p orbital so that not only two but four electrons are available for bonding (note that electrons in full orbitals, i.e., occupied by two electrons, cannot form bonds). From this excited state, i.e., one electron in the 2s orbital and three in 2p orbitals ($2p_x$, $2p_y$ and $2p_z$) (see Fig. 2.4 center), orbital hybridizations can occur, i.e., orbitals mix with each other. Orbitals have three possibilities to combine: either the 2s orbital mixes only with one 2p orbital, they form then the so-called sp hybridization, or the 2s orbital mixes with two (or three) 2p ones, they then form the sp^2 (or sp^3) hybridization.

In the case of graphene (single carbon sheet, see Fig. 2.3 bottom left) or graphite (plenty of graphene sheets on top of each other bounded with weak Van der Waals forces, see Fig. 2.3 right), the 2s electron of carbon forms sp^2 hybridization with both the $2p_x$ and the $2p_y$ electrons (see Fig. 2.4 right column). These resulting three electrons located in sp^2 hybrid orbitals can form bonds with sp^2 electrons of three neighbor carbon atoms, called σ bonds, i.e., overlap of two sp^2 orbital cone ends. All the orbitals try to obtain as much space as possible, which leads to the planar structure of sp^2 hybridized carbon based materials, with an angle of 120° between three consecutive atoms. The remaining 2p electron of each atom occupies the non-hybridized $2p_z$, which is perpendicular to the σ bonds plane. The $2p_z$ electrons also form bonds between carbon atoms, however, the overlap of the orbitals occurs side-by-side. Consequently, these bonds, called π bonds, are not as strong as the σ bonds. They form a delocalized π network which is responsible for electronic transport (see Fig. 2.5).

In carbon nanotubes, the sp^2 hybridization, as related in graphene and graphite, is predominant whereas the sp^3 hybridization also exists due to quantum confinement and topological constraints created by the CNT tubular form [15]. The fraction of sp^3 hybridization increases with a decreasing CNT diameter.

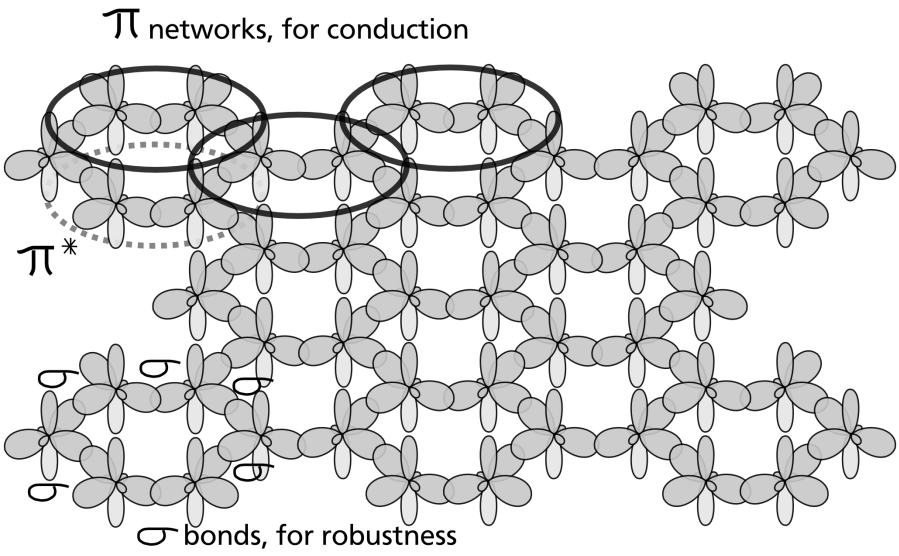

Figure 2.5: σ and π bonding of carbon by graphite, graphene and carbon nanotubes.

"Hexagonal honeycomb" is sufficient to describe entirely the structure of graphene. Unlike this, the structure of SWNTs has to be more precisely specified, as there are many ways to roll up the honeycomb lattice. Only two integers, typically called (n,m) are enough to describe entirely the structure of one SWNT. They represent a node within the graphene lattice. This description appeared for the first time in the publication of Hamada et al. from NEC Corporation in Japan [7]. The origin of the hexagonal lattice of graphene (i.e., the point with (0,0) as coordinates) must be arbitrarily chosen and two unit vectors need to be defined. The definition of Hamada et al. is somewhat different than the one used nowadays by the scientific community. Hamada et al. used vectors which make an angle of 120°. Today, an angle of 60° is more common. For the sake of clarity, the definition used in this work is based on unit vectors making an angle of 60°, called $\overrightarrow{a_1}$ and $\overrightarrow{a_2}$ (see Fig. 2.6). The two integers (n,m) are brought together in the so-called *chiral vector*:

$$\overrightarrow{C} = n\overrightarrow{a_1} + m\overrightarrow{a_2} \tag{2.1}$$

The nanotube is **virtually** formed by the rolling up of the graphene sheet along the direction perpendicular to the direction of the chiral vector. The length of the chiral vector corresponds to the circumference of the nanotube, given in 2.2, where a_{C-C} is the carbon-carbon bond length, a_{C-C}=1.44 $\AA$:

$$circumference = \sqrt{3}a_{C-C}\sqrt{n^2+mn+m^2} \tag{2.2}$$

The diameter of the nanotube is given in equation (2.3):

$$d_{SWNT} = \frac{circumference}{\pi} = \frac{\sqrt{3}a_{C-C}\sqrt{n^2+mn+m^2}}{\pi} \tag{2.3}$$

The picture of rolling up the graphene sheet is very helpful to understand the SWNT structure

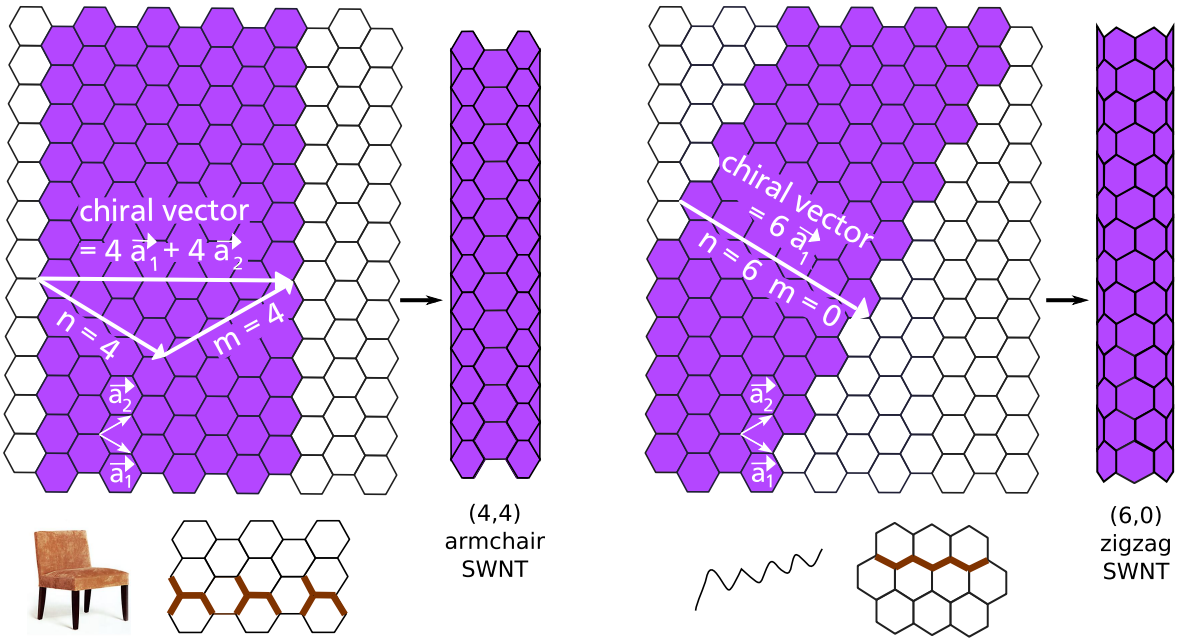

Figure 2.6: Example of armchair SWNT (left) and zigzag SWNT (right).

but does not describe the way SWNTs are formed in reality during their growth process. SWNTs grow from the beginning using the first carbon atoms as tubes.

2.2.3 Metallicity

The Japanese researchers Hamada et al. did not only show how to describe precisely any SWNT, they also classified them into three groups according to their symmetry, computed the band structure of some examples of SWNTs and developped a theory on their metallicity [7]. Their results, true for all SWNTs expect for SWNTs with very small diameters, are reported below.

SWNTs can be classified into three groups according to their geometry: the *armchair*, the *zigzag* and the *chiral* SWNTs. Armchair SWNTs have both integers equal to each other. In this case two opposite C-C bonds are perpendicular to the SWNT axis (see Fig. 2.6 left). Zigzag SWNTs have one of both integers equal to 0. In this case two opposite C-C bonds are parallel to the SWNT axis (see Fig. 2.6 right). Chiral SWNTs represent all the other possible combinations of (n,m). Chiral SWNTs do not have any C-C bonds which are parallel or perpendicular to the tube axis. SWNTs can also be classified into three other groups, this time according to their electrical properties. Indeed, one of the most interesting but also complicated feature of SWNTs is that even a minor change in the diameter can imply a major change in the metallicity, i.e., a SWNT can become a metal, a quasi-metal or a semiconductor. For all SWNTs expect for SWNTs with very small diameters (see next section), the two integers also enable to ascertain the SWNT metallicity.

To understand the metallicity of SWNTs, their electronic band structure need to be computed. A short history on the discovery of the SWNT band structure is given below whereas the major results of its computation are summarized in the next subsection.

Mintmire et al. reported first on the calculation of the band structure of one SWNT [6]. However, their results gave only the electronic structure of one special case of SWNTs, namely the (5,5) armchair SWNT. Using two different methods of calculation, they demonstrated that this SWNT is metallic. The important result is that the conductivity is shown to be very high, comparable to conventional metals ($\sim 10^{22}$ cm^{-3}) and much higher than the conductivity of graphite ($\sim 10^{18}$ cm^{-3}). Armchair SWNTs are a very good conductive material at room temperature even without doping. Several months later, Hamada et al. also computed the band structure of several examples of SWNTs [7], as already mentioned. For this, they first determined the atomic relaxation of the carbon atoms in SWNTs. Atomic relaxation of carbon occurs in SWNTs as opposed to the ideal structure of graphene because of the non-symmetry caused by the curvature of the tubes. Indeed, the σ bonds parallel to the axis of the tube are different to the bonds which are perpendicular or tilted to the tube axis. This difference is absent in graphene because it is a planar structure. The non symmetry of parallel and perpendicular bonds by SWNTs causes stress on atoms. The relaxed structure is obtained after the atoms moved so that there is no stress anymore on them. Hamada et al. calculated this atomic relaxation by using the calculations of Tersoff on the interatomic potential of carbon [16]. They then applied the tight-binding model to compute the band structure of several SWNTs (see subsection 2.2.4). As a result, they demonstrated firstly that armchair SWNTs are always metallic, secondly that SWNTs, for which the difference between n and m is a multiple of 3 (exclusive 0), are quasi-metallic and thirdly that the remaining SWNTs (i.e., for which (n-m)$\neq$3) are semiconducting. This result was compatible with that of Mintmire. Unfortunately the details of their calculation are not presented in their paper. At the same time, Saito et al. also reported on the calculation of the band structure of SWNTs, for armchair and zigzag nanotube originally [17], and later for the remaining ones [18]. Their calculations are based on the band structure of graphene and on the boundary conditions imposed by the tubular form of SWNTs. Table 2.1 summarizes the different groups of SWNTs, according either to their geometry or to their metallicity. Only the armchair group corresponds to the group of purely metallic SWNTs. Zigzag and chiral tubes can be either semiconducting or quasi-metallic.

m and n	SWNT name	metallicity
$n = m$	armchair	metallic
$n = 0 \cap m = 0$	zigzag	depending on n-m
$m \neq n \cup m \neq 0 \cup n \neq 0$	chiral	depending on n-m
$n\text{-}m = 3k, k \in \mathbb{Z}^*$	-	quasi-metallic
$n\text{-}m \neq 3k, k \in \mathbb{Z}$	-	semiconducting

Table 2.1: Metallicity of SWNTs according to their integers (n,m). $\mathbb{Z}$ represents the set of integers, $\mathbb{Z}$ the set of non-zero integers.

The fact that SWNTs have a different metallicity according to their (n,m) integers is something new and very interesting for the scientific community. However, this is also a problem for evident reasons: Metals and semiconductors are not going to be used in the same devices or in the same way and it should be possible to separate them. Unfortunately, it is very difficult to achieve the selective fabrication of s-SWNTs over m-SWNTs (or vice versa) and the separation of s-SWNTs versus m-SWNTs according to their diameter is also impossible. To illustrate this problem, Table 2.2 lists all possible SWNTs with a diameter between 0.950 and 1.059 nm. In

Fig. 2.7, these SWNTs are identified by their node on the graphene lattice, corresponding to the (n,m) integers. There are a total of 13 SWNTs with a diameter of 1 nm ±5% (SWNTs with (n,m) and (m,n) integers are considered as equal and counted only once). Only one SWNT is an armchair and thus purely metallic. Four SWNTs are quasi-metallic and eight tubes are semiconducting. The (7,7) and (6,8) SWNTs have a diameter of 0.961 nm and 0.964 nm respectively but the first is purely metallic and the second semiconducting. This example illustrates the problem of the separation of SWNTs with different metallicity. A selection only based on diameter measurements will most likely not give good results because a tiny difference of 0.3 $\AA$ makes a major change in the electrical characteristics.

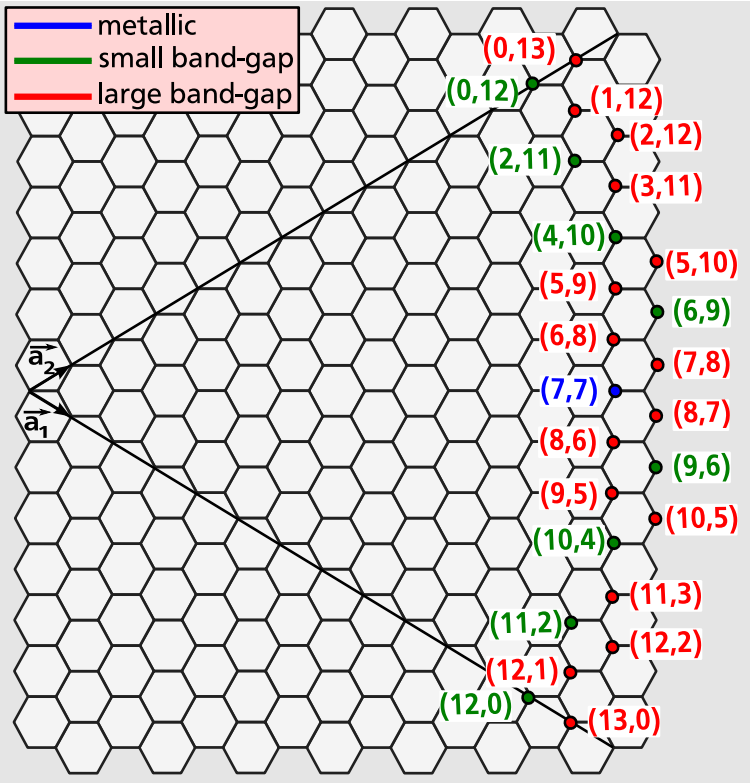

Figure 2.7: Graphic representation of all SWNTs with a diameter between 0.950 and 1.059 nm.

m	n	Diameter (nm)
n	m	
0	13	1.030
0	12	0.951
1	12	0.993
2	12	1.039
2	11	0.961
3	11	1.012
4	10	0.990
5	10	1.049
5	9	0.974
6	9	1.036
6	8	0.964
7	8	1.030
7	7	0.961

Table 2.2: Corresponding diameters.

2.2.4 Band structure

The band structure of SWNTs, especially of s-SWNTs, is very important for the understanding of the operation of carbon nanotube field-effect transistors (see section 2.3). Prior to the calculation of the band structure of SWNTs, some terms like Fermi level, conduction band and valence band, must be defined. For this, a short summary of the band theory of solids is given below.

Some basics of solid state physics [19]

As already mentioned, the energy of electrons belonging to free individual atoms can only take discrete values, called energy states. They correspond to shells, subshells and orbitals. In

solids, atoms interact collectively so that all shells, subshells and orbitals are energetically very close to each other and the allowed energy levels of one electron are multiplied and form nearly continuous bands of energy states. When no energy is applied to the solid (at 0 K), some of these bands are completely filled with electrons and others are empty. The full band with the higher energy is called *valence band* whereas the empty band with the lowest energy is called *conduction band*. The energy difference between the lower state of the conduction band and the upper one of the valence band is called energy *band gap*, abbreviated with E_g ("energy gap"). Only semiconductors and insulators have a band gap. For semiconductors, this band gap is fairly narrow (e.g. ∼1 eV) so that at room temperature some valence band electrons can occupy the conduction band. For insulators, the band gap is very wide. For metals, the valence and conduction bands are overlapping so that there is no band gap.

Electrons have half integer spin and are thus fermions, i.e., particles that obey the Fermi-Dirac statistics. The Fermi-Dirac statistics gives the probability f for an energy state E to be occupied by an electron. It is expressed in equation (2.4), where k is the Boltzmann constant, T the temperature in Kelvin and E_F the Fermi energy or *Fermi level*.

$$f_{Fermi-Dirac}(E) = \frac{1}{e^{(E-E_F/kT)}+1} \tag{2.4}$$

The Fermi level is the energy level at which a state has a 50% probability of being occupied by an electron for T > 0 K. For T = 0 K, E_F represents the highest energy level filled with electrons. For intrinsic (undoped) semiconductors and insulators, the Fermi level is centered within the band gap. The *work function* of a solid is defined by the energy needed to extract an electron from the Fermi level to the vacuum level so that it can freely move.

In quantum mechanics, electrons are regarded as propagating waves. Waves are always represented within the so-called reciprocal space by wave vectors whose module has the dimension of the inverse of a length. If $\vec{a}_1$, $\vec{a}_2$, $\vec{a}_3$ are the unit vectors of the real space, the definition of the unit vectors of the reciprocal space ($\vec{b}_1$, $\vec{b}_2$, $\vec{b}_3$) is given in equation (2.5).

$$\begin{cases} \vec{a}_1 \bullet \vec{b}_1 = 2\pi & \vec{a}_1 \bullet \vec{b}_2 = \vec{a}_1 \bullet \vec{b}_3 = 0 \\ \vec{a}_2 \bullet \vec{b}_2 = 2\pi & \vec{a}_2 \bullet \vec{b}_1 = \vec{a}_2 \bullet \vec{b}_3 = 0 \\ \vec{a}_3 \bullet \vec{b}_3 = 2\pi & \vec{a}_3 \bullet \vec{b}_1 = \vec{a}_3 \bullet \vec{b}_2 = 0 \end{cases} \tag{2.5}$$

To calculate the allowed energy states of electrons in an atom or a solid, the Schrödinger's equation (independent of the time) must be solved for the whole system. The Schrödinger's equation is expressed in equation (2.6).

$$H\,\psi(\vec{k}) = E(\vec{k})\,\psi(\vec{k}) \tag{2.6}$$

H is the Hamiltonian, $E(\vec{k})$ and $\psi(\vec{k})$ the eigenvalues and eigenfunctions of the energy of the system at wave vector $\vec{k}$. The electronic band structure of a solid represents the allowed energy states of electrons with their corresponding wave vectors ($\vec{k}$). It is an energy versus a wave vector, or more exactly versus its projections on the three axis (k_x, k_y, k_z). Crystals are mostly three dimensional structures. Since there is no way to plot an energy versus a three dimensional space (four dimensions!), the energy is usually plotted as a function of $\vec{k}$ along certain lines of

symmetry within the first Brillouin zone (unit cell of the reciprocal space). This leads to a two dimensional graph.

For semiconductors, the boundaries of the valence/conduction bands are not necessarily constant for all wave vectors. At particular wave vectors, the boundaries of the bands reaches a minimum for the conduction band and a maximum for the valence band. If the maximum and minimum are reached at identical $\overrightarrow{k}$ values, the semiconductor is called a direct semiconductor. If not, the semiconductor is called an indirect semiconductor. The energy difference between the valence band maximum and conduction band minimum defines the band gap. For indirect semiconductors, the band gap is calculated from the projection, since the energies are taken at different wave vectors. Only direct semiconductors can emit photons which are created via electron-hole recombinations. Silicon for instance is an indirect semiconductor and cannot emit light. As an illustrating example, the electronic band structure of silicon is given in Fig. 2.8,

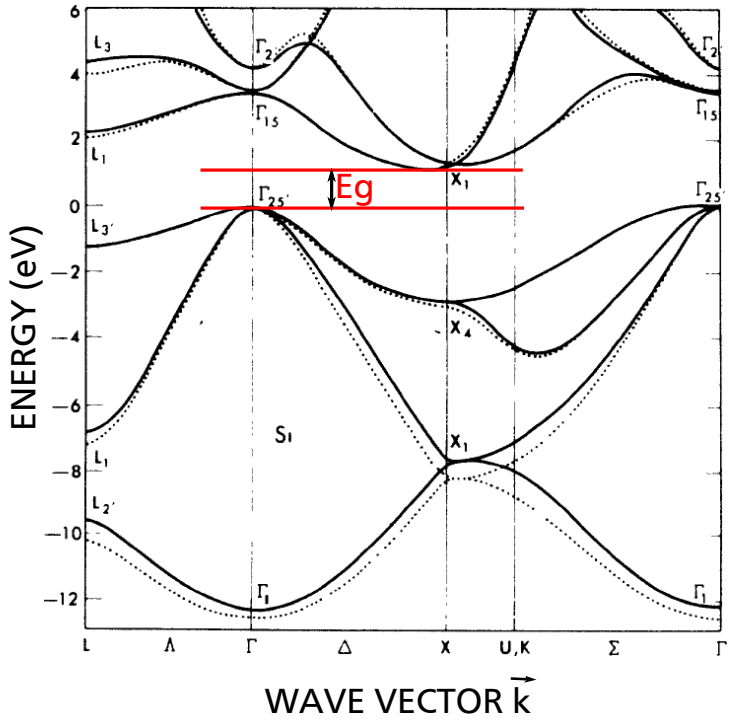

Figure 2.8: Electronic band structure of silicon along the lines of symmetry within the first Brillouin zone from [20]. The circles emphasize the indirect band gap.

where the indirect band gap can be seen.

Graphene band structure

Back to the band structure of SWNTs: The band structure of graphene must first be computed since the SWNT band structure is based on graphene. It is not possible to solve Schrödinger's equation for all electrons of graphene without doing some simplifications. Two common simplifications which are used:

1. Electrons are considered as free particles, which move almost like in a gas, and feel weakly the potential created by the atoms of the lattice. Since atoms are arranged periodically to form a crystal, the potential felt by electrons is also periodic. Electrons are described as plane waves [21].

2. Electrons are considered as part of the atoms of the solid [21]. This is called tight-binding approximation and is used for solids in which atoms are sufficiently close to each other so that the overlap of the atom wave functions is strong enough to necessitate an adjustment of the result obtained on isolated atoms but not strong enough to make the description of the energy states of the atom completely irrelevant for the solid [19]. This model is applied mostly to transition metals where the d-shells are only partly filled and for insulating materials [19].

The second simplification is known to work remarkably well for graphene [21]. Already in 1947, Wallace published the computation of the electronic band structure of graphene using the tight-binding model [22]. It is supposed that the conduction in graphene is only based on electrons in the p_z orbital, i.e., the non-hybridized orbital which is oriented perpendicular to the graphene lattice (see subsection 2.2.2). These electrons are independent from the other valence electrons and form the π-bond network of graphene (see Fig. 2.5). Usually, band structures are calculated within the first Brillouin zone (unit-cell of the reciprocal space). Fig. 2.9 shows the graphene lattice in the real space. The unit vectors of the real space are $\vec{a}_1$ and $\vec{a}_2$. The first

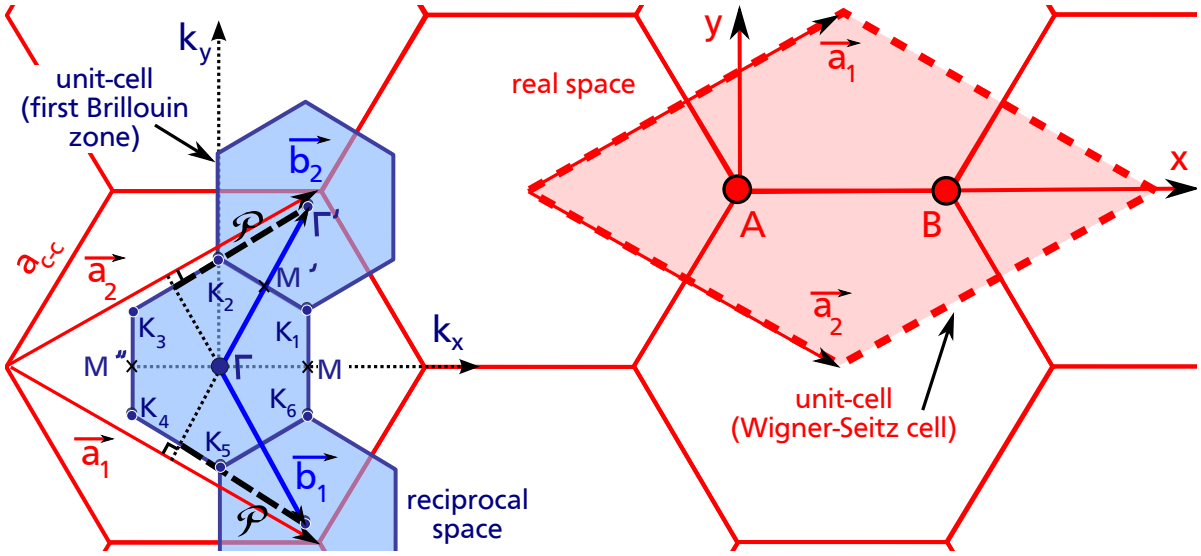

Figure 2.9: Schematic of graphene in the real and reciprocal spaces.

Brillouin zone is also shown, this time drawn in the reciprocal space. The unit vectors of the reciprocal space are $\vec{b}_1$ and $\vec{b}_2$, constructed according to the set of equations (2.5). In the two dimensional case, the equations are equivalent to the set of relations (2.7), where $\mathscr{P}$ is the projection of $\vec{b}_1$ on $\vec{a}_1$ (also of $\vec{b}_2$ on $\vec{a}_2$, see Fig. 2.9) and a the length of the unit vectors ($\sqrt{3}a_{C-C}$).

$$\begin{cases} \vec{b}_1 \perp \vec{a}_2 \\ \vec{b}_2 \perp \vec{a}_1 \\ \mathscr{P} = 2\pi/a \end{cases} \tag{2.7}$$

The first Brillouin zone of graphene is hexagonal as is the structure in real space, and has three specific points: the K points (apexes of the hexagon), the M points (middles of the hexagon sides) and the Γ point, center of the hexagon.

When solving the Schrödinger's equation (2.6) with the nearest-neighbor tight binding approximation, the electronic band structure of graphene is given in equation (2.8) [18, 22], where γ_0 is the nearest-neighbor overlap integral. "Nearest-neighbor" means that only the influence of the nearest-neighbor atoms on electrons is taken into account.

$$E_{2D}(k_x, k_y) = \pm\gamma_0 \left\{ 1 + 4\cos(\frac{\sqrt{3}k_x a}{2})\cos(\frac{k_y a}{2}) + 4\cos^2(\frac{k_y a}{2}) \right\}^{\frac{1}{2}} \tag{2.8}$$

Because graphene is a two dimensional structure, the wave vector $\overrightarrow{k}$ is replaced by its projections only on the x and y axes k_x and k_y respectively. Unlike silicon, the projection on the z axes is equal to 0 so that the band structure can be plotted as a three dimensional graph with the z axis representing the energy. Inserting equation (2.8) in a program for drawing graphs [23], the electronic band structure of graphene can be drawn as the example shown in Fig. 2.10. The π^*

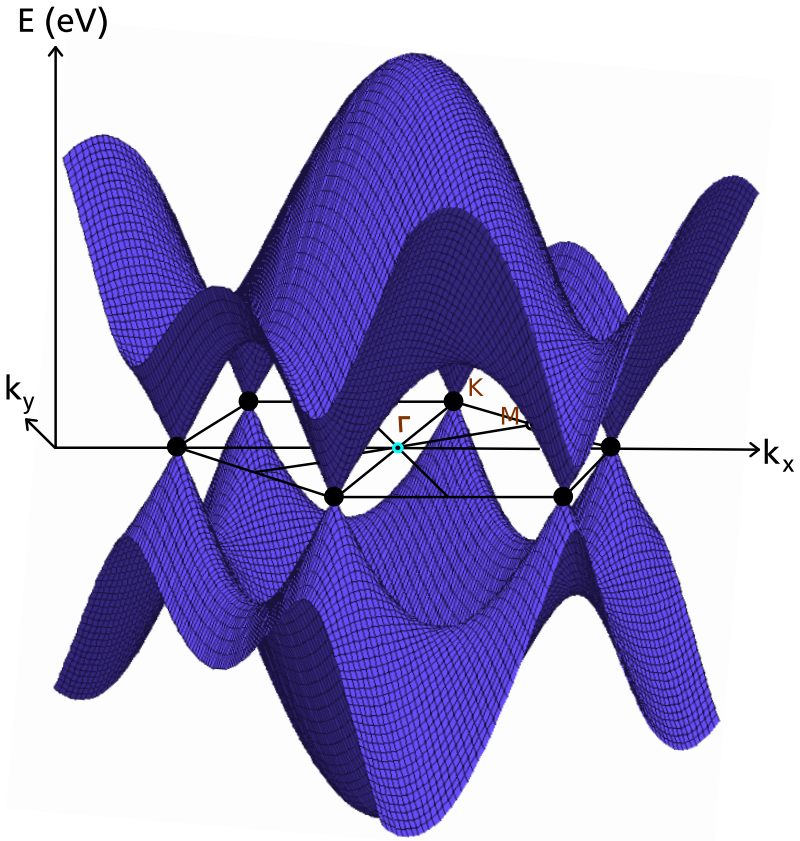

Figure 2.10: Graphene band structure. This graphic has been computed with the program Archim [23].

valence band (bottom) and the π conduction band (top) do not have any common surfaces but six common points. These six points correspond to the six apex of the hexagonal first Brillouin zone of graphene (K points). The energy level of these six points corresponds to the Fermi energy of graphene. Graphene is not a semiconductor because there is not a real energy range (i.e., band gap) which is completely free from allowed wave vectors. On the other hand, graphene is also not a real metal because conduction and valence bands do not have any common points at most wave vectors. These are properties of a so-called semi-metal. The metal characteristics are obtained only at the wave vectors near the K points.

Method to deduce SWNT band structure

The electronic band structure of SWNTs can now be deduced from the one of graphene. For this procedure, the so-called zone folding approximation is used, which means roughly that the electronic band structure of graphene is cut into "pieces" of allowed wave vectors. The superposition of the sliced parts of the graphene electronic structure forms the SWNT electronic band structure. The selection is based on supplementary boundary conditions induced by SWNTs.

Graphene is assumed as a planar surface, periodic and infinite in both directions of the plane. This infers that the wave vector is continuous in both directions of the plane. SWNTs also have a periodic infinite structure along the tube axis, but in the transverse direction (direction of the chiral vector), the structure is finite. This implies a quantization of the wave vector along the transverse direction, whereas the wave vector along the tube axis is continuous as for graphene. In the zone-folding approximation related here, the SWNT tubular form is neglected, i.e., SWNTs are considered as a planar structure, infinite in the direction of the tube axis, periodic in the transversal direction. The period of the transversal direction is the circumference of the tube (length of the chiral vector), depending only on (n,m) (see equation (2.2)). The quantization of the transversal direction is then equivalent to the one dimensional case of an electron in a periodic potential, a well-know problem in quantum mechanics. The condition which the wave function should obey is given in equation (2.9) where L is the period of the potential, here, the circumference of the SWNT and $\psi(x)$ is the planar linear progressive wave describing the electron:

$$\psi(x) = \psi(x+L) = \psi(x+circumference) \quad \text{with} \quad \psi(x) = A\exp^{ikx} + B\exp^{-ikx} \tag{2.9}$$

The well known result of this boundary condition is:

$$k = \frac{2p\pi}{circumference}, \quad p \in \mathbb{Z} \tag{2.10}$$

which means that the component of the SWNT wave vector along the direction of the chiral vector can only take discrete values (points). Since the component along the tube axis is continuous, the authorized wave vectors for all SWNTs form lines which are parallel to the tube axis, as depicted in Fig. 2.11 left. Fig. 2.11 center shows these lines on the electronic band structure of graphene. For the sake of clarity, only the positives energies have been represented. The two dimensional SWNT band structure is plotted as follows: each line of authorized wave vectors which crosses the first Brillouin zone is used as the x axis, and each corresponding energy graph is drawn on each other. An example of SWNT band structure is given in Fig. 2.11 right. Important for the determination of the metallicity of the tubes is where exactly these lines cross the first Brillouin zone. Indeed, when the lines cross the K points, then the K-points belong to the authorized wave vectors and the SWNT is metallic. If not, the SWNT has a band gap for all its allowed wave vectors, which means that it is semiconducting.

Armchair SWNT band structure

For armchair SWNTs, n=m implies that the angles between chiral vector $\overrightarrow{C} = n\overrightarrow{a_1} + m\overrightarrow{a_2}$

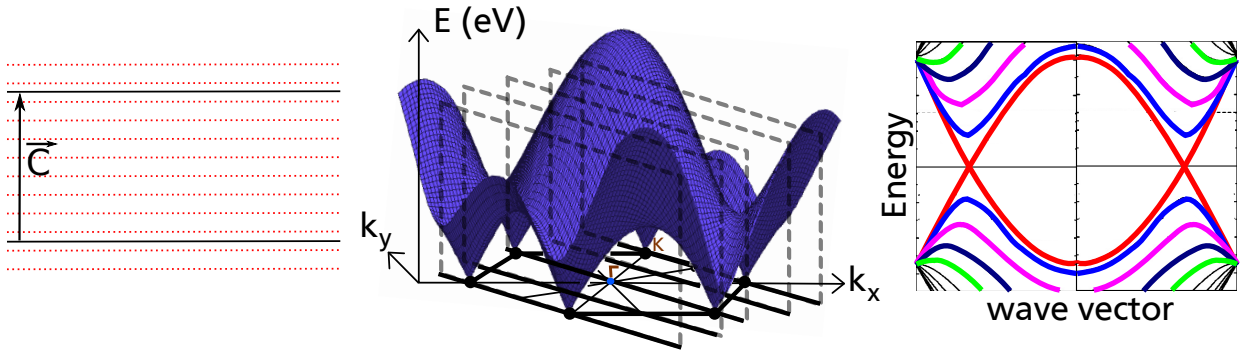

Figure 2.11: Left: Representation of an infinite SWNT in the plane and its quantized wave vectors. Center: Illustration of SWNT supplementary quantization on graphene 2D band structure. Right: Example of SWNT band structure (adapted from [24]). Each color represents another line of authorized wave vectors.

and both unit vectors $\overrightarrow{a}_1$ and $\overrightarrow{a}_2$ are the same. Looking at Fig. 2.9, this means that the chiral vector is along $\overrightarrow{k_x}$. The authorized lines are then oriented perpendicular to $\overrightarrow{k_x}$, i.e., parallel to $\overrightarrow{k_y}$. From "n=m" and equations (2.2) and (2.10), the condition of quantization for armchair SWNTs can be deduced, as detailed in equation (2.11).

$$k_x = \frac{2p\pi}{circumference} = \frac{2p\pi}{\sqrt{3}a_{C-C}\sqrt{n^2+mn+m^2}} = \frac{2p\pi}{3a_{c-c}n} = \frac{p}{n}\frac{2\pi}{3a_{c-c}}, \quad p \in \mathbb{Z} \tag{2.11}$$

When observing Fig. 2.9, elementary geometrical considerations lead to the result that K_2 and K_5 belong to the lines of authorized wave vectors when $k_x = 0$, K_1 and K_6 when $k_x = \Gamma M$ and K_3 and K_4 when $k_x = -\Gamma M$. The distance ΓM is calculated in equation 2.12.

$$\Gamma M = \Gamma\Gamma'/2 = \frac{\mathscr{P}}{\cos 30°} = \frac{2\pi/a}{\cos 30°} = \frac{2\pi}{3a_{c-c}} \tag{2.12}$$

From equations (2.11) and (2.12), $k_x = 0$ is true when p=0, $k_x = \Gamma M$ when p=n and $k_x = -\Gamma M$ when p=-n. Since p is an integer, it is in fact always true, which means that the six K-points always belong to the authorized wave vectors. Accordingly, the armchair tubes are always metallic. This result is illustrated in Fig. 2.12. On the left, the allowed wave vectors of the (6,6) SWNT are drawn on the first Brillouin zone of graphene. The six K-points belong to lines of wave vectors. On the right, the band structure of the SWNT is given from [7]. The point where no energy gap exists can be easily identified. For a better appreciation of this sweep, Fig. 2.12 center shows the graphene band structure from the $[K_1K_6]$ perspective, where the Γ, X and K_3 are indicated. Γ and M are coincident, as well as K_6 and K_4 and lastly K_1 and K_3.

Zigzag SWNT band structure

For zigzag tubes, one of the integers is equal to zero, so that the chiral vector is along one of the unit vectors, i.e., along one side of the hexagon of the Brillouin zone. Two new wave vector directions are introduced, $k_\perp$ and $k_{//}$, as illustrated in Fig. 2.13a left. The allowed wave

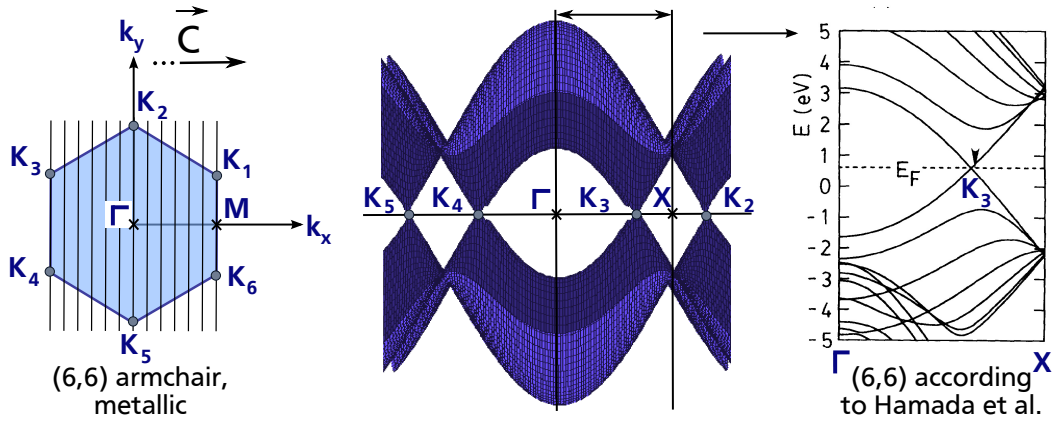

Figure 2.12: Left: Allowed wave vectors lines of (6,6) SWNT. The gray points indicate when a wave vector line crosses a K point. Center: view of graphene band structure as seen from the $[K_1K_6]$ perspective. Right: Band structure of (6,6) SWNT from [7].

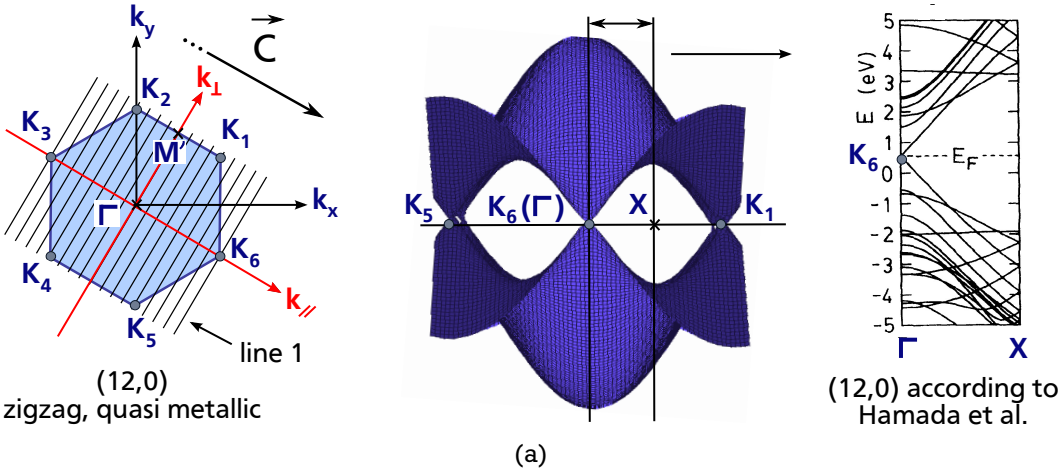

(a)

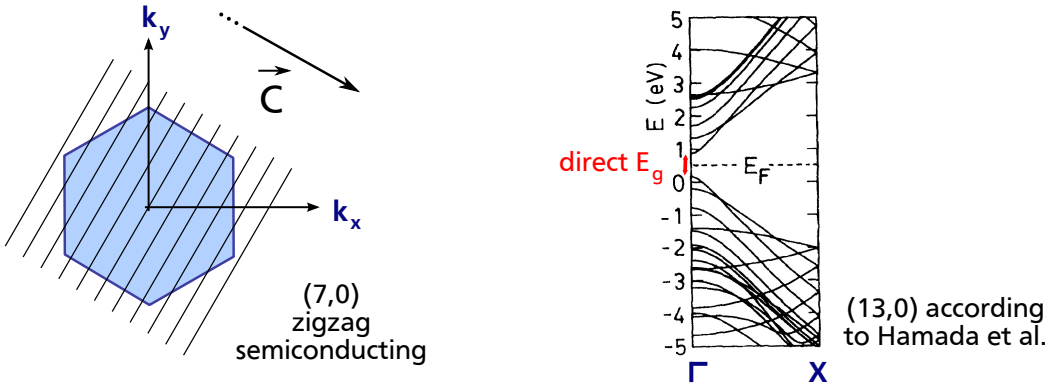

(b)

Figure 2.13: (a): Left: allowed wave vectors of (12,0) SWNT. The gray points indicate when a wave vector line crosses a K point. Middle: view of graphene band structure "as seen from line 1". Right: Band structure of (12,0) SWNT from [7]. (b): Left: allowed wave vectors of (13,0) SWNT. No allowed wave vector line crosses a K point. Right: Band structure of (13,0) SWNT from [7].

vector lines are oriented along $k_{\perp}$, i.e., the boundary condition is along $k_{//}$. From "m=0" and equations (2.2) and (2.10), the condition of quantization for zigzag SWNTs can be deduced:

$$k_{//} = \frac{2p\pi}{circumference} = \frac{2p\pi}{\sqrt{3}a_{C-C}\sqrt{n^2+mn+m^2}} = \frac{2p\pi}{\sqrt{3}a_{c-c}n} = \frac{3p}{n}\frac{2\pi}{3\sqrt{3}a_{c-c}} \tag{2.13}$$

Once again, elementary geometrical considerations lead to the result that K_3 and K_6 belong to the lines of authorized wave vectors when $k_x = \pm\Gamma K_6$ and $K_{1,2,4,5}$ when $k_x = \pm M'K_1$. In equations (2.14) and (2.15), the distances ΓK_6 and M'K_1 are calculated respectively. From equations (2.13), (2.14) and (2.15), it can be deduced that if p takes the value 2n/3 and n/3, the zigzag SWNT will be metallic.

$$\Gamma K_6 = \frac{\Gamma M}{\cos 30^\circ} = 2\,\frac{2\pi}{3\sqrt{3}a_{c-c}} \tag{2.14}$$

$$[M'K_1] = [\Gamma K_1\ \sin 30^\circ] = \frac{2\pi}{3\sqrt{3}a_{c-c}} \tag{2.15}$$

As p is an integer, n should be a multiple of three to obtain metallic tubes. This is e.g. the case of the (12,0) SWNT whose allowed wave vectors are drawn in Fig. 2.13a left and electronic band structure from [7] given in Fig. 2.13a right. In Fig. 2.13a center, a view of the band structure of graphene seen from the "line 1" perspective is drawn where X, Γ and the K-points are represented. This perspective helps to understand the band structure of the (12,0) SWNT represented on the right. Γ, K_6 and K_3 are coincident, as well as K_5 and K_4 and lastly K_1 and K_2.

If n is not a multiple of three, the lines of allowed wave vectors do not cross any K point at all. The SWNT is then purely semiconducting. Fig. 2.13b shows the lines of the (7,0) SWNT and the computed band structure of the (13,0) SWNT taken from [7]. For the sake of clarity, a (7,0) SWNT and not a (13,0) has been drawn. The valence and conduction bands are separated by a forbidden range of energy for all wave vectors. At the Γ point, the lowest possible energy of the conduction band and the highest possible energy of the valence band are reached simultaneously, which is the definition of a direct band gap. Note that the wave vector line giving this band gap is not the one crossing the Γ point (in the middle of the Brillouin zone) but the one at the end of the Brillouin zone.

Chiral SWNT band structure

The integers of chiral SWNTs obey the following rules: n≠m, n≠0, m≠0. With a similar method as for zigzag tubes, it can be shown that chiral SWNTs are metallic only if (n-m) is a multiple of three (non zero). Fig. 2.14 gives two examples of chiral SWNTs, on the left, the metallic (6,3) SWNT and on the right the semiconducting (7,3) SWNT.

Accuracy and limitations of the previous approximation for SWNT band structure

The fact that SWNTs can be metallic or semiconducting according to their chirality, despite their similarity in structure makes them a really novel and unique material. The zone folding of the nearest neighbor tight binding model of graphene is a very elementary approach to cal-

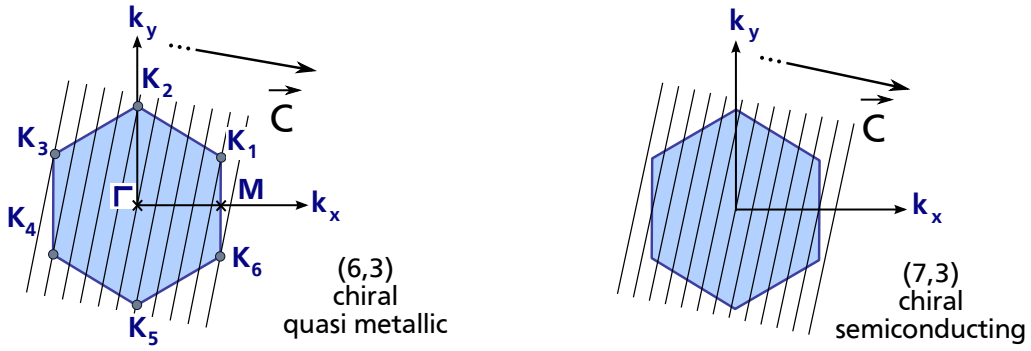

Figure 2.14: Left: allowed wave vectors of (6,3) m-SWNT. The gray points indicate when a wave vector line crosses a K point. Right: allowed wave vectors of (7,3) s-SWNT. No allowed wave vector line crosses a K point.

culating the band structure of SWNTs and the easiest one, in fact. Nevertheless, in most cases it provides a good approximation of the SWNT band structure and reasonably correct information on the SWNT metallicity. However, the experimental results sometimes differ from the theoretical approximation:

1. Zigzag and chiral tubes are only quasi metallic and not purely metallic, which does not appear in Fig. 2.13 and Fig. 2.14. The quasi metallic feature of SWNTs should not be confused with the semi-metal feature of graphene, coming from its Fermi level which is reduced to singularities. Quasi metallic SWNTs are actually semiconducting but with a very narrow band gap, so that their behavior is much closer of the metallic one. The reason is that for all the calculations reported above, the changes in the structure, which are induced by the curvature, have been neglected. SWNTs have been considered as a periodic plane and not as a tube. However, the curvature implies a change in the distance between atoms: the carbon hexagon is not perfect anymore. This change in the structure (atomic relaxation, see also previous section) is responsible for the narrow band gap found experimentally by zigzag and chiral tubes even when the difference (n-m) is a multiple of three. In contrast, armchair tubes are not affected by this phenomenon due to their symmetry and are really purely metallic.

2. The method of the folding of the graphene band structure assumes that all the C-C bonds in SWNTs comes from the sp^2 hybridization of the carbon atomic orbitals, whereas the electrical conduction comes only from the non-hybridized vertical 2p orbital, as in the case for graphene. However, the strong curvature of SWNTs implies a rehybridization of the carbon orbitals. This can be neglected by large diameter SWNTs, locally almost planar, whereas it plays an important role in small diameter SWNTs whose curvature is very strong [25]. The hybridization is then a mixture of sp^2 and sp^3 and the band structure of such SWNTs cannot be deduced anymore from the one of graphene.

For "large diameter" SWNTs ($\geq$1 nm), the description based on the zone folding of graphene reported previously is applicable and, moreover, it enables the computation of a relation between s-SWNT band gap and diameter. White et al. obtain the equation (2.16) based on the first order development of the graphene band structure equation (2.8) in a Taylor series approximation [26].

$$E_g = 2.7\ eV \frac{0.142\ nm}{radius\ in\ nm} = \frac{0.8}{diameter\ in\ nm} eV \tag{2.16}$$

The dependency of the SWNT electronic band structure with SWNT geometry has not only been demonstrated many times theoretically, but also observed experimentally at the atomic scale by Odom et al. from Harvard [27]. Fig. 2.15 shows two examples of their results, taken from their paper which appeared in 1998 in Nature. In Fig. 2.15a, the atomic structure of a metallic SWNT as well as its I-V characteristic on the nanometer scale is represented, whereas in Fig. 2.15b, the same comparison for a semiconducting SWNT is given. Differences in the structure as well as in the electrical sweep are clearly visible, confirming the theory.

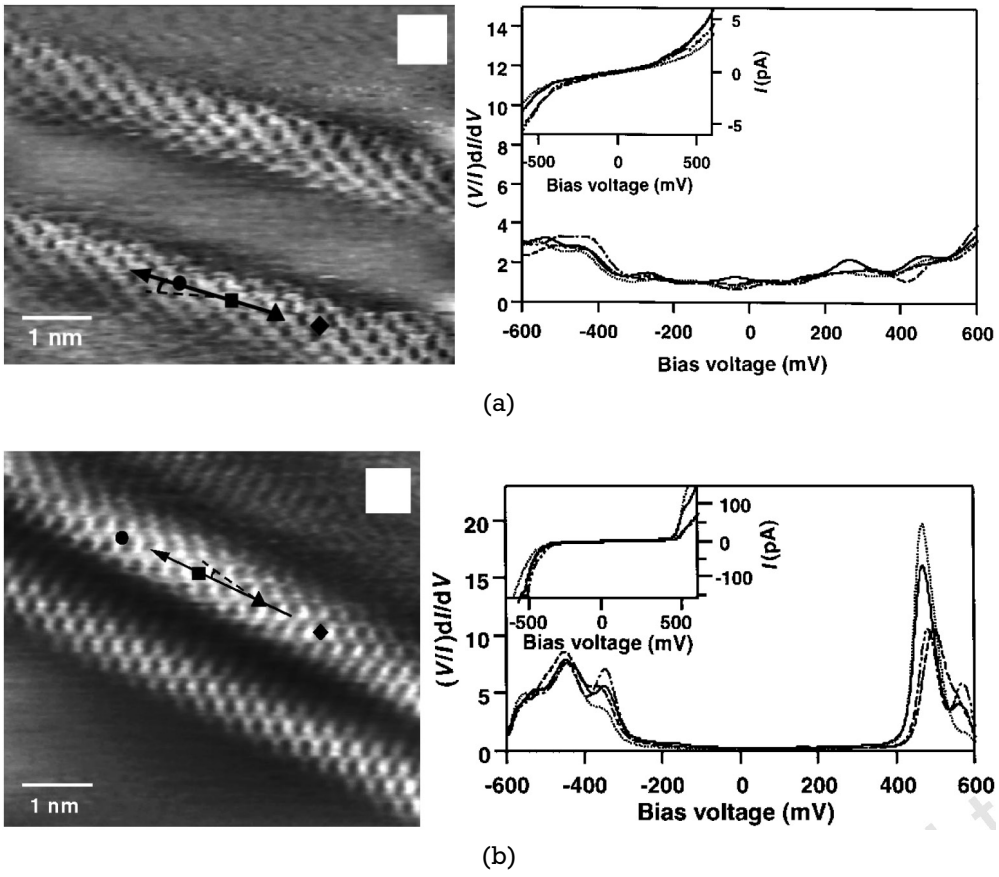

Figure 2.15: Results from Odom et al. [27]. (a): STM scan of a metallic SWNT (left). I-V measurement (inset). Deduced normalized conductance (right). The measurement occurred at the position indicated by the symbols. (b): The same for a semiconducting SWNT.

2.2.5 Electronic transport

In SWNTs, the electronic transport is known to be ballistic. A ballistic transport occurs in a finite semiconductor when the length of the conductive path (e.g. distance between two electrodes) is shorter than the mean free path of electrons, so that electrons move through the material without any scattering process. The mean free path of electrons is the mean distance between two scattering processes. White and Todorov, who published on the first theoretical calculations which prove that SWNTs can be ballistic conductors, obtained a result of at least 10 μm for the mean free path of armchair tubes [28].

In CNT structures, ballistic transport is possible due to the unique one-dimensional tubular structure in which electrons move along the tube axis without backscattering. However, the conductivity of the tubes has an absolute maximum as in all one dimensional transport systems. The one dimensional subbands of nanotubes form one dimensional conduction channels that have the conductivity of a conductance quantum ($G_0 = 2q^2/h$, with q the elementary charge and h the Planck constant) leading to the nanotube intrinsic conductivity of $4q^2/h$ (due to the spin degeneracy) [29]. This means that a maximal conductivity of 155 μS or a minimal resistance of 6.5 kΩ can be reached. In any case, the minimal resistance is in practice almost never attained due to parasitic additional contact resistances. In CNTFETs, some reports indicate that the choice of an appropriate metal, like Pd, as well as an adapted structure like short channel, lead to resistances in the on-state, the values of which are near the theoretical limit [30, 31].

2.2.6 Synthesis methods

There are three major possibilities to synthesize single-walled carbon nanotubes: arc discharge, laser ablation and *in situ* catalytic chemical vapor deposition (CCVD):

1. When Iijima observed for the first time carbon nanotubes under an SEM in 1991, the growth method used was *arc discharge* [1]. This method was initially developed for the production of fullerenes. Two carbon sticks, used as electrodes, are placed about 1 mm far apart from one another, within an inert gas at low pressure. A current of 50 A passes through the electrodes and causes the vaporization of the graphite. The carbon then condenses on the cathode, part of it in the form of carbon nanotubes. To obtain the growth of SWNTs, cobalt [8] or nickel must be added to the anode. The arc discharge method has the advantage of being simple but the disadvantage that CNTs are mixed with other products of the reaction and need to be purified after growth.

2. *Laser ablation* was introduced in 1996 by Guo et al. [32]. A laser is used to vaporize a graphite target in which cobalt and nickel are added. The major advantage over arc discharge is the improvement of the yield. The proportion of CNTs to other products increases to 70% in weight. The vaporization of graphite occurs at 1200°C in argon, followed by heat treatment in a vacuum at 1000°C to remove the C_{60} molecules and other fullerenes.

3. The last possibility of growing CNTs is actually a very established method: *chemical vapor deposition* of carbon which comes from a gas, such as a hydrocarbon, like methane. The CVD process cannot occur alone, it needs a catalyst to break the gas molecule, commonly a transition metal like iron, cobalt or nickel. Important is the form and size of the catalyst, which has to be nanometer-scale clusters. Nanotubes grow from these catalytic particles, at low or atmospheric pressure, under temperatures in the range of 600-1000°C. The great advantages of the CVD method are the following:
   - the lower process temperature
   - no need to purify the CNTs from the soot
   - the possibility of using this method directly on silicon wafer to avoid subsequent manipulation of CNTs after growth [33]
   - the possibility of controlling the density and size of nanotubes by controlling the size of the clusters.

2.3 Carbon Nanotube Field-Effect Transistor (CNTFETs)

A *field-effect transistor* (FET) is a device which controls the current flow via the electric field. The two states of the transistors, i.e., on- and off-states, are characterized by their currents (*on-current* and *off-state leakage current* or *off-current*). There are many ways to build an FET. The *MOSFET* (Metal Oxide Semiconductor Field-Effect Transistor) is probably the best known FET. It is a silicon based device which has three main electrodes: source and drain between which the current flows and gate which is situated on top of the gate oxide. The gate electric field allows (or inhibits) the formation of a conductive channel within the silicon between source and drain regions. Very often, CNTFET operation is assumed to be directly equivalent to MOSFET properties, because of marked similarities: The current flows between source and drain electrodes, and is controlled by the electric field created by the bias applied to the gate electrode which is electrically separated from S/D with an insulating layer. Moreover, the resulting sweeps of CNTFETs and MOSFETs look fairly similar. However, the nanotube transistors present some important differences, due to the fact that CNTs replace bulk silicon as the channel material. First, the unique one-dimensional form of the SWNTs implies a ballistic transport over hundreds of nm at room temperature whereas scattering occurs in MOSFETs even for devices with a 10 nm gate length [34]. Moreover, all C-C bonds in SWNTs are chemically saturated, whereas dangling bonds on the surface of silicon induce energy states within the band gap at the interface Si/gate oxide. The Si/SiO_2 interface is considered to be nearly perfect. However, when fabricating MOSFETs with high-κ dielectrics directly on Si (e.g. Gd_2O_3), carrier mobility usually degraded due to an imperfect interface [35]. This problem is absent in CNTFETs since the CNT channel has saturated bonds.

In the following section, a short review on metal-semiconductor contacts is given, since they play a major role in the CNTFET operation. Subsequently, a description of the CNTFET operation is given.

2.3.1 Metal-semiconductor contact

At a metal/semiconductor contact, a potential barrier is formed at the interface. When applying a bias between metal and semiconductor, the barrier is either reduced (forward direction) or increased (reverse direction) at the semiconductor side, according to the polarity of the bias. At the metal side, the barrier height does not change. When the potential barrier is higher than 3kT (0.78 eV at room temperature) in the reverse direction, it prevents most carriers from passing through the contact which is called rectifying or *Schottky contact*. The barrier is usually called *Schottky barrier*, or Schottky barrier height (SBH). As a result, the junction conducts a non-negligible current for the forward polarity but not for the reverse polarity, this is the reason why the metal-semiconductor contact is also called Schottky-diode. The current voltage characteristic is highly non-linear.

At moderate temperature (e.g. room temperature) and for moderately doped semiconductors, *thermionic emission* is the predominant process for conduction through Schottky contacts [36]. The magnitude of the thermionic current depends only on the barrier **height**. To pass through the junction, the carriers should have a sufficiently high energy to overcome the Schottky barrier, which is the case when the temperature is sufficiently elevated. At low temperature, no thermionic emission is possible.

Theoretically, the SBH for electrons is the difference between the semiconductor conduction band lower edge and the metal Fermi level, i.e., the SBH depends ideally on the metal work function. Accordingly, the SBH for holes is ideally the difference between the semiconductor valence band upper edge and the metal Fermi level.

Ohmic contacts between a metal and a semiconductor are obtained in three cases:

• when there is basically no Schottky barrier for both bias polarities. When using the ideal definition for SBH given above, the absence of a barrier can also be referred to a negative Schottky barrier, i.e., the difference between the semiconductor conduction band lower edge (valence band upper edge) energy level and the metal Fermi level is negative.

• when the barrier is sufficiently low ($\leq$3kT) for both bias polarities.

• when the barrier depletion zone is extremely thin, e.g. Al/Si-n^+ contacts. Actually, when the barrier depletion zone is very narrow, another conduction mechanism called tunneling injection of carriers is predominant in metal-semiconductor junctions [36]. Tunneling is a phenomenon in quantum mechanics. To pass through the junction, carriers do not need to overcome the potential barrier, but since they also have wave properties, a certain probability for them to tunnel through the barrier exists. The thinner and lower the barrier, the higher the probability for carriers to tunnel through. In highly doped semiconductors, the Schottky barrier becomes very thin so that the probability for carrier tunneling is high and independent of bias polarity, making an ohmic contact of the metal-semiconductor junction.

In ohmic contacts, the current-voltage characteristic is linear for **both** bias polarities. Good ohmic contacts should also have a low resistance in relation to the total resistance of the semiconductor device.

For planar Si or Ge, or other covalent semiconductors in contact with a metal, the SBH deviates experimentally from the expected one: the SBH does not directly depend on the metal work function. This phenomenon is called *Fermi level pinning*. The Fermi level pinning originates from the fact that the atoms at the interface semiconductor/metal have a different structure than the bulk ones because of e.g. some damaging at the surfaces of the materials, or, when the contact is very good, new chemical bonds between the two materials. The Fermi level pinning is then often attributed to interface states, i.e., new possible energy levels which are situated within the band gap of the semiconductor, due to boundary conditions. These states only depend on the semiconductor bulk structure making the SBH independent of the metal work function [37]. However, some phenomena are not fully explainable, for example the variations of the SBH between the same metal/semiconductor pair. New studies have demonstrated that Fermi level pinning can be explained in term of polarization of chemical bonds at the metal/semiconductor interface [38]. The SBH depends on the one hand on the semiconductor structure and on the other hand, not on the metal work function but on the quality of the interface, and amongst others, on the orientation of the metal layer [39].

For covalent semiconductors in contact with metals, the reduction of the Schottky barrier height is complicated due to Fermi level pinning. Ohmic contacts for Si-based devices can be obtained more easily via tunneling using highly doped semiconductors (see above).

2.3.2 CNTFET operation

For SWNT devices, it is possible to adjust the Schottky barrier height easily since the one-dimensional nanometer scale geometry of the tubes reduces drastically the Fermi level pinning

phenomenon. The SBH for electrons depends simply on the difference between the metal work function and the bottom edge of the conduction band, the SBH for holes depends on the difference between the metal work function and the top edge of the valence band [40]. The adjustment of the SBH opens the possibility to develop CNTFETs which work as Schottky barrier FETs [41], with the special cases of ohmic contacts CNTFETs (OC-CNTFETs) [30] and mid gap CNTFETs.

Another possibility to build CNTFET is to use p/n junctions of doped CNT-material to realize S/D contacts as in conventional MOSFETs to avoid the Schottky barrier [42]. In these so-called MOS-CNTFET devices, the SWNT acts as the channel and also as source/drain junctions. The end parts of the tube are doped and used as S/D extensions, whereas the middle of the tube, which is not doped, serves as the channel [42]. These structures show very good performances at elevated supply voltages [43]. However, they are difficult to produce, more practicable to fabricate are SB-CNTFETs. The operation of these devices is described in detail below.

The first published results on fully functional devices were all based on SB-CNTFETs. In 1998, Tans et al. from the Delft University of Technology in The Netherlands [44], almost simultaneously with Martel et al. from IBM [45] reported on the first fully functional CNTFETs. Heinze et al. published in 2002 the first demonstration that CNTFETs work as Schottky barrier FETs [41]. The operation of SB-CNTFETs is based on the modulation of the Schottky barrier via the electric field, to control the passage of the carriers through it, in addition to the modulation of the channel conduction.

In Schottky contacts, the conduction is mainly based on majority carriers [36]. However, in most publications as well as in the experiments presented later in this work, the SWNTs are not doped, i.e., they are used as intrinsic semiconductors. Thus, electrons and holes can participate in the conduction through the metal-semiconductors contacts. Schottky barriers for both holes and electrons should be considered. According to the metal used as S/D electrodes, the diameter of the SWNT and the sort of carriers which are considered, three kinds of Schottky barrier exist in CNTFETs:

- High and wide Schottky barriers: They prevent both thermionic emission at room temperature and tunneling injection of carriers.
- High but narrow Schottky barriers: The contact is ohmic since carriers can tunnel through it. The current is proportional to V_{ds}.
- Low, 0 eV or even negative Schottky barrier: The contact is ohmic.

A very important feature of CNTFETs is that the width of the Schottky barrier at the SWNT-metal contact is found to depend mainly on the gate oxide thickness [41].

Three theoretical examples of SB-CNTFETs are given below, where a 1 nm diameter SWNT serves as the channel (average diameter of SWNTs grown in this work, see chapter 3). The first example deals with ambipolar SB-CNTFETs, the second case is a p-type CNTFET fabricated with palladium as S/D material and the third example is a n-type CNTFET with aluminum S/D electrodes. Lastly, some concluding remarks on CNTFET operation are given.

The value of 4.7 eV is taken for SWNT work function ($q\phi_{SWNT}$), based on the study of Shan and Cho [46], who have shown that all SWNTs with a diameter above 0.8 nm have a work function near that of graphene (4.66 eV). SWNT band gap (E_g) is calculated with equation (2.16): 1 nm diameter leads to 0.8 eV. χ_{SWNT}, the electron affinity of SWNTs, defined as the bottom edge of the conduction band, is given in equation (2.17). The Schottky barriers are supposed to be ideal, i.e., calculated as difference between $q\phi_M$ (metal work function) and top edge of valence band (for holes)/electron affinity (for electrons), as indicated in equation (2.18) for electrons

and (2.19) for holes [36]. When applying a gate voltage, the barrier width can be reduced or increased according to the polarity of the bias.

$$q\chi_{SWNT} = q\phi_{SWNT} - E_g/2 = 4.3\ eV. \tag{2.17}$$

$$\text{SBH for electrons } = q\phi_{Bn} = q(\phi_M - \chi_{SWNT}) \tag{2.18}$$

$$\text{SBH for holes } = q\phi_{Bp} = E_g - q(\phi_M - \chi_{SWNT}) \tag{2.19}$$

In the following examples, the voltage applied to the source is always equal to 0 V whereas the voltage applied to the drain is either equal to ±400 mV or to -1 V. Note that the two cases obtained at $V_{ds} = \pm 400$ mV are not symmetrical and represent two different electronic configurations, since the source is always equal to 0 V.

Ambipolar CNTFET

Ambipolar is the common name given to CNTFETs which have significant currents for both sufficient positive and negative gate voltages, i.e., the transistors are n and p-type [47]. The off-state region of such transistors is reduced to a narrow gate voltage range of around 0 V. This is due to the fact that undoped SWNTs are used which behave as intrinsic semiconductors, and both hole conduction ($V_{gs} < 0V$) and electron conduction ($V_{gs} > 0V$) are possible, when the Schottky barriers are favorable for both conductions. Three cases of ambipolar CNTFETs are known: CNTFETs with ultra down-scaled gate oxide thickness allowing carriers tunneling, CNTFETs with large diameter SWNTs which present reduced SBH due to the reduced SWNT band gap, and mid gap CNTFETs (even with thick oxide) [35]. The description, band profile and conduction mechanisms of mid gap CNTFETs are given below.

Mid gap refers to the special case of SB CNTFET in which the Fermi level of the S/D metal is located nearly in the center of the SWNT band gap, i.e., work functions of both SWNT and metal are identical: $q\phi_M = q\phi_{SWNT} = q\chi_{SWNT} + E_g/2$. From equation (2.18) and (2.19), it is evident that in mid gap CNTFETs, the barriers for electrons and holes are identical in magnitude. The metal and SWNT parameters of the mid gap CNTFET considered here are summarized in Table 2.3. From these parameters, the band profile of a metal/SWNT/metal contact can

SWNT diameter	d_{SWNT}	1 nm
SWNT band gap	E_g	0.8 eV
SWNT work function	ϕ_{SWNT}	4.7 V
SWNT electron affinity	χ_{SWNT}	4.3 V
Metal work function	ϕ_M	4.7 V
SBH for electrons	ϕ_{Bn}	0.4 V
SBH for holes	ϕ_{Bp}	0.4 V

Table 2.3: Parameters of mid gap CNTFET

be drawn, as shown in Fig. 2.16. Usually, when contacts are formed between a metal and

a semiconductor with different work functions, an adjustment of their Fermi levels induces a bending of valence and conduction bands of the semiconductor. This does not occur in mid gap CNTFETs because the Fermi levels are already nearly at the same position since both work functions are identical (see Fig. 2.16b). When an electric field is applied to a semiconductor, by applying a gate bias to the gate electrode, the energetic position of valence and conduction bands edges are shifted due to band bending. However, the distance between both, the band gap, stays the same. For negative V_{gs}, the bands are shifted in the positive energy direction, i.e., they become nearer to the vacuum level of the metal. This is illustrated in the case of the mid gap CNTFET in Fig. 2.16c. As a result, the barrier for electrons (difference metal Fermi level - conduction band bottom edge of SWNT) is increased, inhibiting electron conduction, whereas the top of the valence band is now above the Fermi level, which is favorable for hole conduction. The Schottky barrier height does not alter through the application of a positive gate voltage. Only its width is clearly reduced. When applying a positive V_{gs}, the situation is exactly the same, with the only difference that electron conduction would be favorable under appropriate drain-source voltage, whereas hole conduction would be inhibited (see Fig. 2.16d).

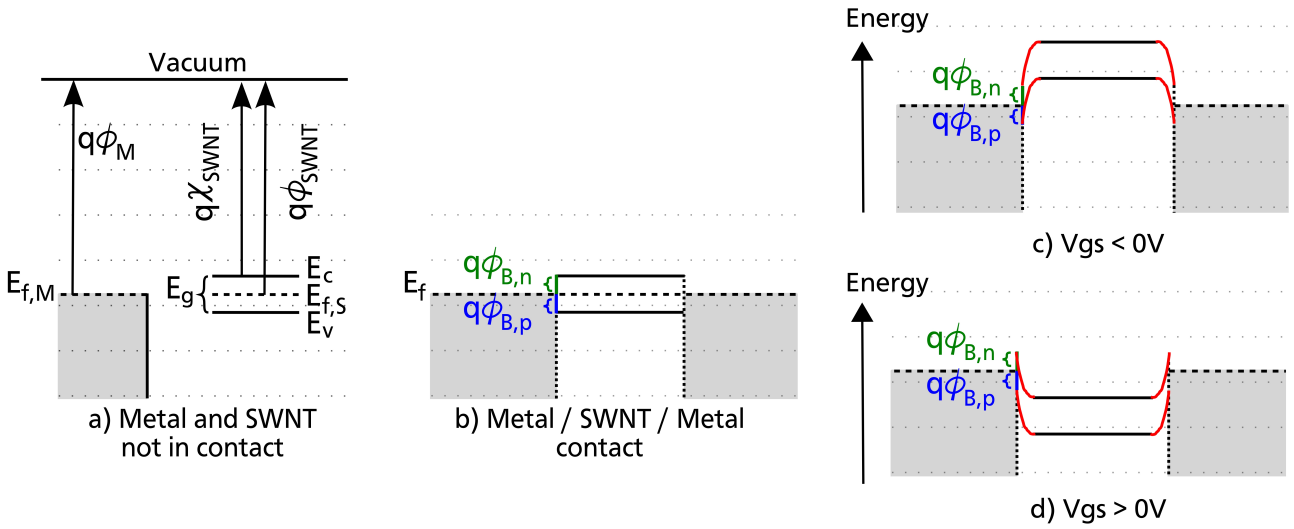

Figure 2.16: Contact formation of a metal/SWNT/metal structure. Metal work function: 4.7 eV. The structure corresponds to a mid gap CNTFET.

Fig. 2.17 shows the band profile for a mid gap CNTFET operating under different V_{ds} (V_s = 0 V, V_d = -400 mV or -1 V). Operating under sufficiently high V_{ds} and negative V_{gs}, conduction of both electrons and holes occur in the mid gap transistor as shown in Fig. 2.17a. For reduced V_{ds}, only hole conduction is possible, as shown in Fig. 2.17b.

For positive V_{gs}, whatever the drain-source voltage, only the conduction of electrons is possible, as shown in Fig. 2.17c. At the metal/SWNT contact (source side), electrons either tunnel or pass above the barrier with thermionic emission. They are then accelerated because the energy of the conduction band bottom edge is much lower than the Fermi level of the metal. The energy accumulated with this acceleration is used to reach the energy of the metal Fermi level at the drain side and finally pass above (or through) the SWNT/metal contact. The conduction mechanism (thermionic emission or tunneling) which occurs in this CNTFET depends on the gate oxide thickness. When the gate oxide thickness is reduced, the Schottky barrier width becomes very narrow, allowing tunneling of carriers through the contacts. When the gate

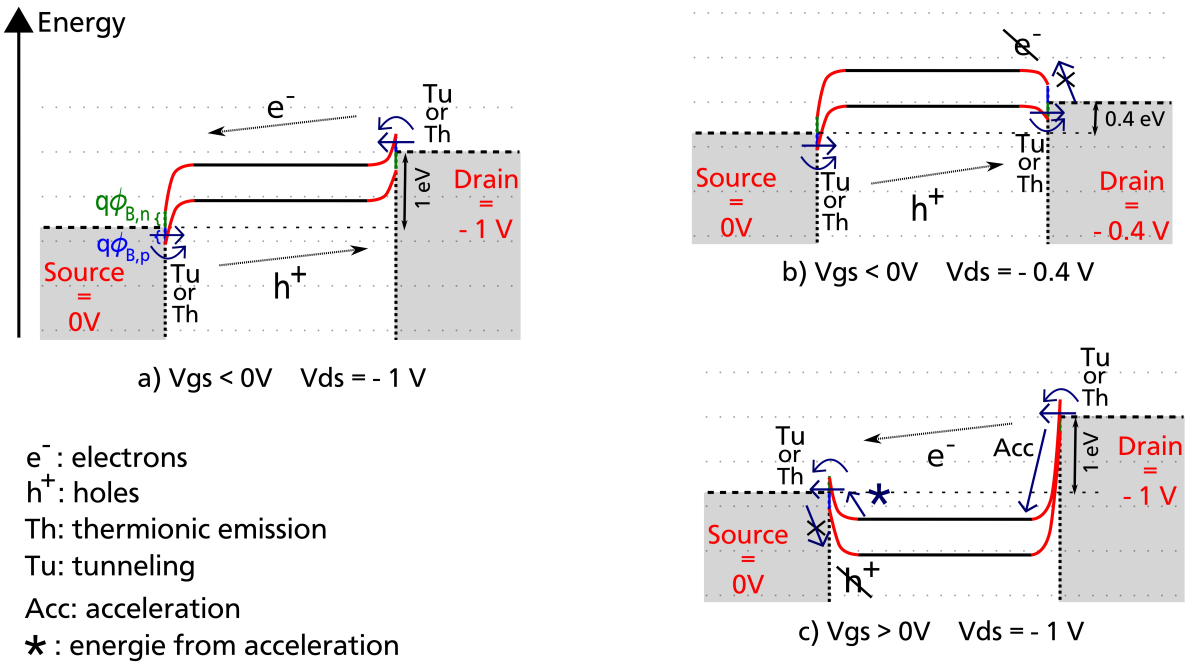

Figure 2.17: Conduction mechanism in mid gap CNTFET.

oxide is fairly thick, tunneling is inhibited and thermionic emission of carriers is predominant. Thermionic emission of carriers highly depends on the temperature. Accordingly, a temperature dependence is expected for thick oxide mid gap CNTFETs. However, since the current density due to hole conduction for negative V_{gs} and electron conduction for positive gate voltage are always approximately identical in a mid gap CNTFET, whatever the gate oxide thickness (i.e., the conduction mechanism), ambipolar electrical characteristics are obtained for any oxide thickness. Even when the gate oxide thickness is reduced, thus reducing the width of the SB to allow tunneling and resulting in a much higher current density at room temperature, this kind of operation for a transistor always leads to a loss of conductivity as a drawback due to the enhanced contact resistance. On the other hand, unipolar transistors are required to replace the conventional MOSFET in CMOS technology.

Ohmic contact CNTFETs

In 2003, Javey et al. published for the first time on Pd-contacted CNTFETs, which they called ohmic contact CNTFETs [30], which are a special kind of SB-CNTFETs. The metal of the S/D electrodes is especially chosen so that one kind of carriers (only electrons or holes) has an SBH almost or exactly equal to 0 eV, or even a negative value. These devices show higher performance than mid-gap SB CNTFETs [48], since ohmic contacts allow higher I_{on}. Moreover, the devices are found to be unipolar (p-type). There is only hole conduction at negative V_{gs} and no electron conduction at positive V_{gs}. To provide ohmic contacts to s-SWNTs, the metal should have either a high work function ($\phi_M \approx \chi_{SWNT} + E_g/2$), allowing a barrier free flow of holes, or a low work function ($\phi_M \approx \chi_{SWNT}$), allowing a barrier free flow of electrons.

P-type CNTFET with Pd S/D electrodes

We consider here a CNTFET contacted with *Palladium* (ϕ_{Pd} = 5.0 eV), and assume a 1 nm SWNT as channel. The resulting barrier for holes, calculated from equation (2.19), is equal to 0.1 V. The parameters of this CNTFET are summarized in Table 2.4. From these parameters, the

SWNT diameter	d_{SWNT}	1 nm
SWNT band gap	E_g	0.8 eV
SWNT work function	ϕ_{SWNT}	4.7 V
SWNT electron affinity	χ_{SWNT}	4.3 V
Metal work function	ϕ_M	5.0 V
SBH for electrons	ϕ_{Bn}	0.7 V
SBH for holes	ϕ_{Bp}	0.1 V

Table 2.4: Parameters of Pd contacted CNTFET

formation of the Pd/SWNT/Pd contact can be drawn, as illustrated in Fig. 2.18 together with the changes occurring when the double contact is maintained under the field-effect. Due to the fairly high Schottky barrier for electrons (0.7 V), the conduction for electrons will be prevented whatever the applied drain-source voltage, except when the Schottky barrier is very narrow. This would happen when the oxide thickness is significantly reduced. At negative gate voltages, hole conduction will be possible when applying a drain-source bias.

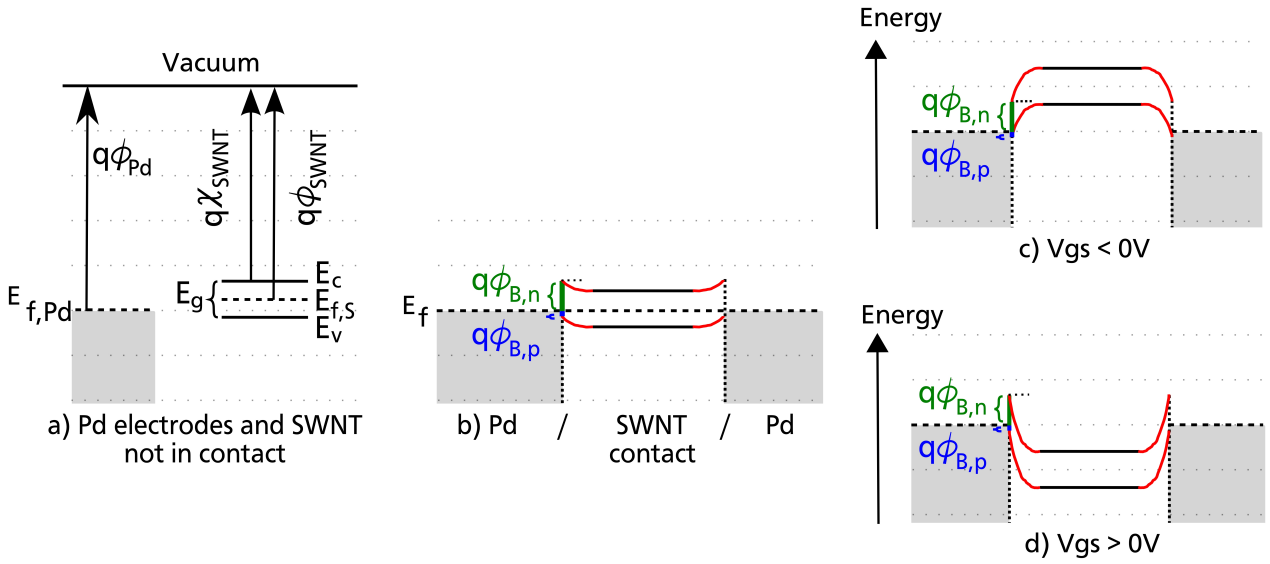

Figure 2.18: Contact formation of a Pd/SWNT/Pd structure.

Fig. 2.19 shows the band profile of the Pd contacted CNTFET when applying a drain-source voltage of ±400 mV. When the upper edge of the valence band is shifted above the Fermi level of metal, i.e., when V_{gs} is negative, holes can go easily from the Pd electrode (drain electrode for V_{ds} = +400 mV / source electrode for V_{ds} = -400 mV) to the SWNT with thermionic emission, since the Schottky barrier for holes is only 0.1 V. This is shown in Fig. 2.19a and c, for V_{ds} of -400 mV and +400 mV respectively. The barrier at the SWNT/Pd contact (drain contact for V_{ds} = -400 mV, source contact for V_{ds} = +400 mV) being smaller for negative V_{ds}, it is expected

that the drain-source current is higher for negative V_{ds} than for the positive V_{ds}. The conduction

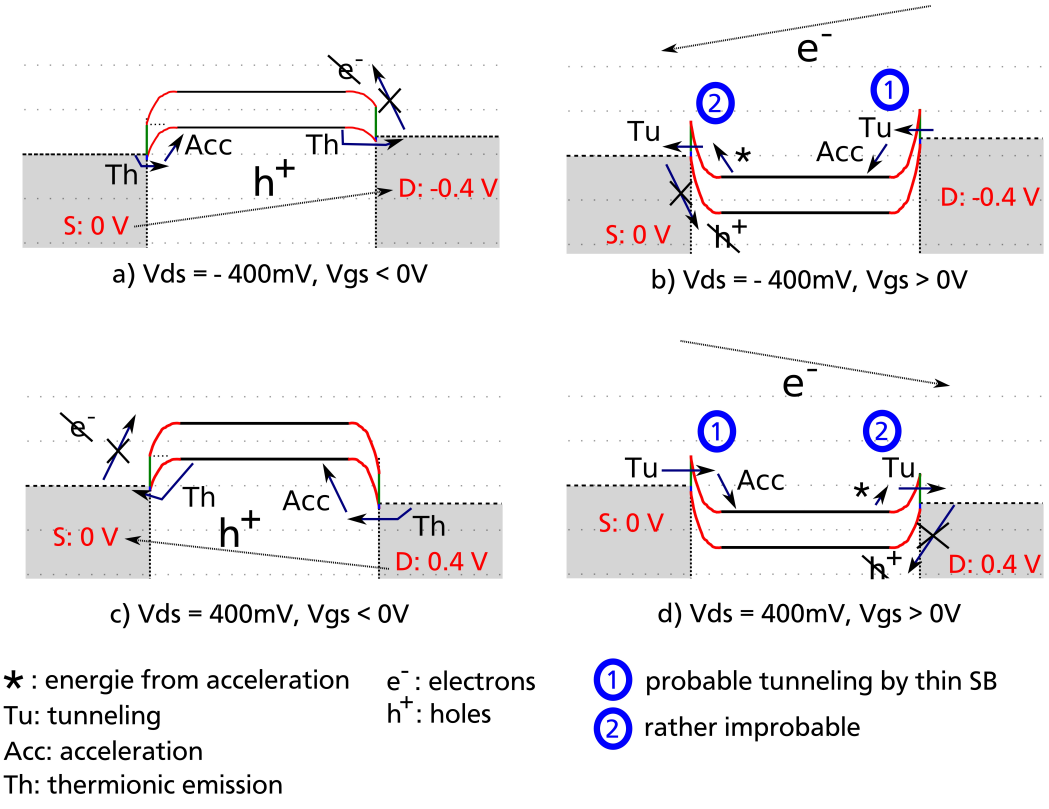

Figure 2.19: Conduction mechanism in Pd contacted CNTFET.

of electrons is shown to be supressed for negative V_{gs}, since the conduction band lower edge is situated considerably over the Fermi level of the metal. More interesting is what happens for positive gate voltages. In this case, the upper edge of the valence band is shifted considerably below the Fermi level of metal, completely inhibiting hole conduction. Electron conduction would be possible but the Schottky barrier is very high (0.7 eV). Thermionic emission is very unlikely in this case, only tunneling through the contact would be predominant, but only if the dielectric is sufficiently thin to reduce the width of the Schottky barrier. This means that the devices are theoretically unipolar (only based on hole conduction at negative V_{gs}) when the dielectric is thick enough. Javey et al. obtain devices perfectly unipolar with a gate dielectric made of 500 nm SiO_2 [30].

N-type CNTFET with Al S/D electrodes

Aluminum with its work function of 4.3 eV is found to be a good metal to produce *n-type* ohmic contact CNTFETs [49, 50]. The parameters of an Al contacted CNTFET with a channel made of a 1 nm SWNT are given in Table 2.5. The Schottky barrier for electrons is exactly equal to 0 V (theoretically): SBH for electrons = $q\phi_{Bn}$ = $q(\phi_M\text{-}\chi_{SWNT})$ = q(4.3-4.3) = 0 V (see equation (2.18)). In the same way as for Pd devices, the contact Al/SWNT/Al is depicted in Fig. 2.20. Hole conduction would be possible only by a very thin Schottky barrier whereas electron conduction is very favorable when V_{gs} is positive.

Fig. 2.21 shows the band profile of an Al contacted CNTFET operating under ±400 mV. Theoretically, the situation is the same as for Pd, but based this time on the conduction of electrons.

SWNT diameter	d_{SWNT}	1 nm
SWNT band gap	E_g	0.8 eV
SWNT work function	ϕ_{SWNT}	4.7 V
SWNT electron affinity	χ_{SWNT}	4.3 V
Metal work function	ϕ_M	4.3 V
SBH for electrons	ϕ_{Bn}	0.0 V
SBH for holes	ϕ_{Bp}	0.8 V

Table 2.5: Parameters of Al contacted CNTFET

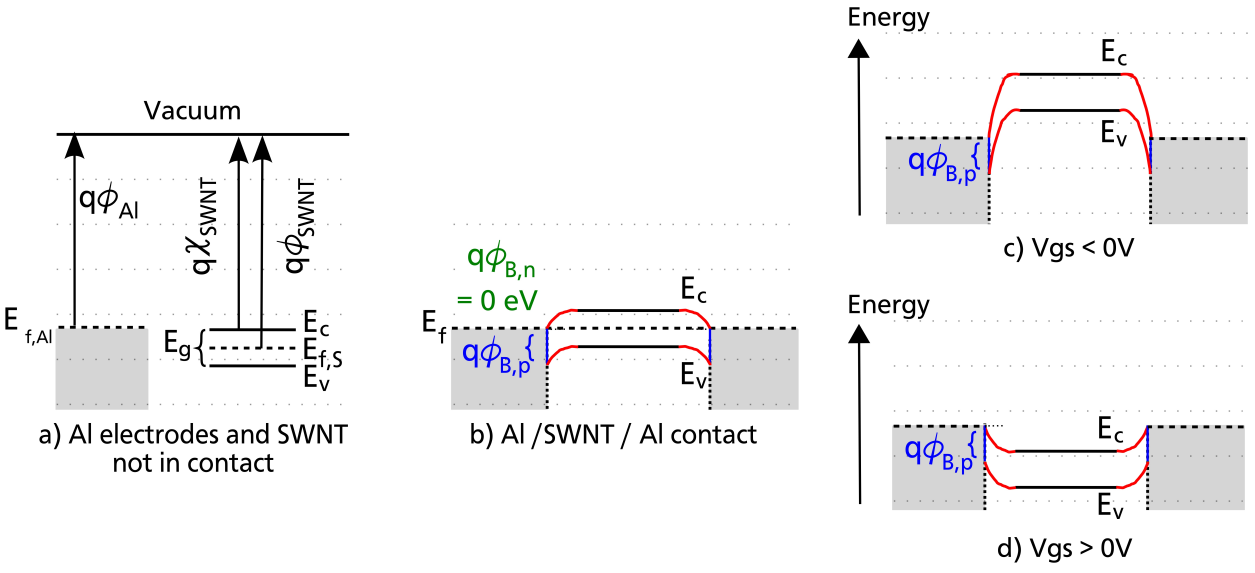

Figure 2.20: Contact formation of an Al/SWNT/Al structure.

Fig. 2.21d shows the best case for conduction, i.e., when V_{ds} and V_{gs} are positive. There is no barrier for electrons at the Al/SWNT contact (source side) and only a tiny one at the contact SWNT/Al (drain side). $V_{ds} < 0$ V also lead to the conduction of electrons, but the magnitude of the current is theoretically reduced compared to $V_{ds} > 0$ V since the barrier is slightly higher. Lastly, hole conduction at negative gate voltages could only be possible if the carriers can tunnel

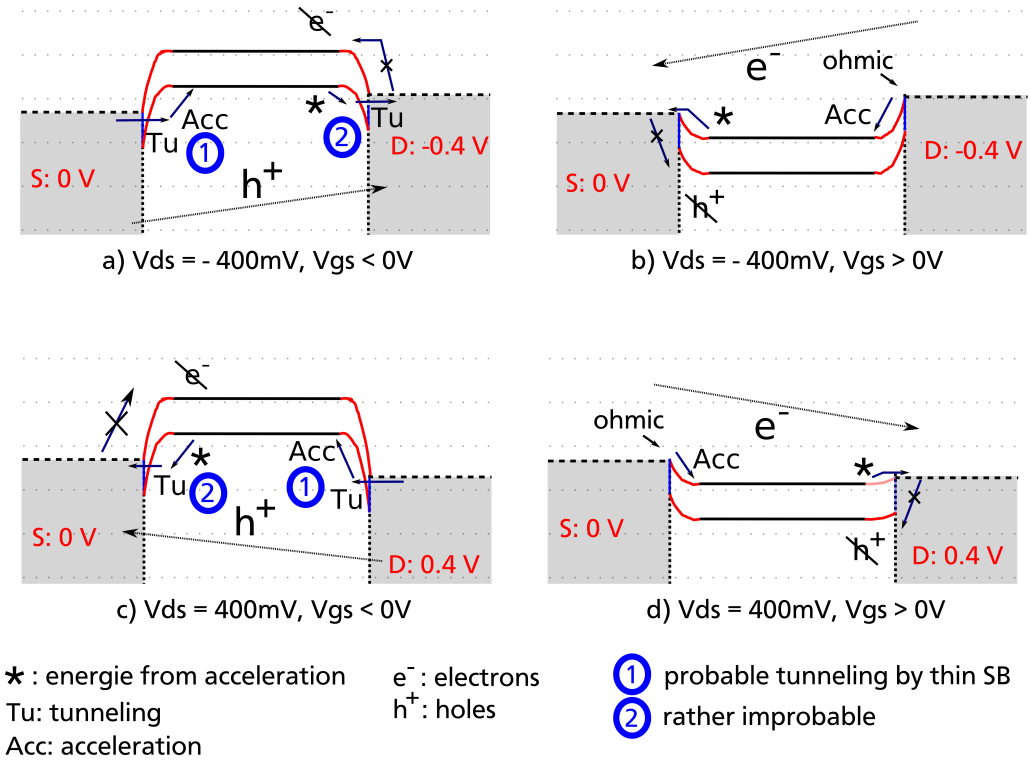

Figure 2.21: Conduction mechanisms in Al contacted CNTFET.

through the Schottky barrier, i.e., for very thin barriers, which are obtained with ultra down-scaled gate dielectrics.

Concluding remarks: Ideal description versus real behavior

From the previous paragraphs, it can be concluded that ultra down scaled dielectrics always lead to an ambipolar behavior of CNTFETs. However, unipolar transistors with ultra down scaled gate oxide are required in order to replace MOSFET with CNTFET in the future. This feature can be achieved by introducing an asymmetry in the source and drain electrodes. With different S/D geometries, e.g. different thicknesses for the bottom oxide at source and drain contacts, different electrostatics are obtained, i.e., large electric field at one contact and small at the other [51]. Appenzeller et al. have shown that carrier tunneling can also be reduced or suppressed by using a double gate structure [52]. Lastly, making source and drain unsymmetrical by using two different metals with different work functions, or different gate-drain and gate-source spacers [53], is also a solution to avoid ambipolar conduction in CNTFETs.

The description of contact formation, SBH and band profiles given above is the easiest way to describe the three possibilities for a CNTFET to work when the contacts are metallic. However, this cannot be applied for all SWNTs and all metals. For instance, Javey et al. report that ohmic

contact operation of their devices is only true for large diameter s-SWNT (>1.6 nm) due to their smaller band gap [30]. Rhodium (Rh) is also found to form ohmic contacts to s-SWNTs, but only for s-SWNTs with a diameter of more than 1.6 nm [54]. Furthermore, platinum for instance, which also has a high work function, is not found to be as suitable as Pd: the transistors work more like SB-CNTFETs than like OC-CNTFETs and show decreased conductivity [30]. One possible explanation for this is given by Shan and Cho [55]. They show that it is not only the work function which has an influence on the SBH between a metal and a s-SWNT but also the atomic geometry: Two metals with same work function but different geometry, e.g. Pd and Pt, lead to different SBH with SWNTs.

Another deviation from the ideal case is the fact that the band profiles have been drawn for intrinsic SWNTs. However, SWNTs may be slightly p-doped under ambient air due to the presence of oxygen. SWNTs are indeed found to be very sensitive to oxygen [56]. This p-doping of SWNTs would explain why usually p-type CNTFETs are obtained under ambient air with all kind of metals, instead of the theoretical type deduced from the band profiles, which could also be n-type or ambipolar. On the other hand, it is possible that not SWNTs but the contact regions are "doped". Pd for instance is known to change its work function in a hydrogen environment. Javey et al. have done an experiment on a Pd contacted CNTFET in which they change the Pd work function *in situ* by exposing the transistor to hydrogen. Increasing H_2 exposure is supposed to reduce the Pd work function and should have an influence on the SBH and thus on the current conduction in the device. They found indeed that the conduction due to holes decreases whereas the one of electrons increases with increased H_2 exposure. This means that the SBH has increased for holes and decreased for electrons. Such "contact doping" could also occur on other metal interfaces in ambient air and explain the deviation between the theoretical band profiles and the experiments. Lastly, Yamada reports on the effect of oxygen on the Schottky barrier height of the metal/SWNT contact [57]. As a conclusion, the scientific community agrees on the fact that oxygen plays an important role in the operation of CNTFET whereas the mechanism of the oxygen influence remains controversial.

2.4 Carbon nanotube applications

For the last ten years, new publications have been appearing permanently on novel applications of carbon nanotubes. This chapter is not going to present an exhaustive list of all CNT-devices already demonstrated. The aim shall only be to emphasize the unique properties of CNTs which allows them to be used in numerous electronic devices and also in sensors. Numerous applications are based on CNTFETs, the main topic of this PhD work, whose operation has been described in the previous section (2.3). Other devices including sensors are only mentioned for completeness.

MWNTs have been used in gas ionization sensors [58]. Flow velocity measurements have been realized with a novel sensor based on bundles of SWNTs [59]. Also, the capacitance of an SWNT network is found to change in presence of diverse chemical vapors [60]. SWNTs bundles and networks are made up of a mixture of semiconducting and metallic ones. The uses of such mixtures are limited.

In contrast, single semiconducting SWNTs are the most interesting carbon nanotube species for electronic devices. They can be used as the active material in PN junctions or metal/semiconductor junctions. They can act as the channel in field-effect transistors (CNTFETs), which

could replace silicon based MOSFETs in the future as the basic part in electronic circuits.

CNTFETs do not only work as conventional FETs, but may also be used as non-volatile memory cells. In 2002, Fuhrer et al. reported on a high-mobility s-SWNT transistor used as a nonvolatile charge-storage memory element operating at room temperature [61]. The s-SWNT is directly used as the readout, based on the hysteresis in the transfer characteristics of the FET. The hysteresis is the horizontal shift between the two sweeps measured respectively at V_{gs} increasing and decreasing and is a typical phenomenon in CNTFETs. In chapter 5, the operation of such a memory cell is described in more detail since the CNTFETs fabricated within this PhD have been measured successfully as non-volatile memory as well.

Moreover, CNTFETs can work as sensors for numerous quantities. For example, Kong et al. show that the threshold voltage of CNTFET transfer characteristics changes within an NH_3 or NO_2 environment (see Fig. 2.22a) [62]. A change in the threshold voltage always corresponds

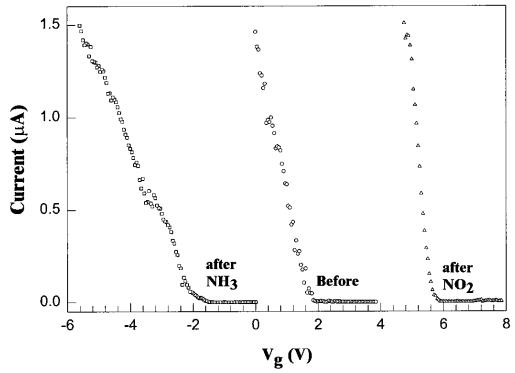

(a) Gas sensor [62]

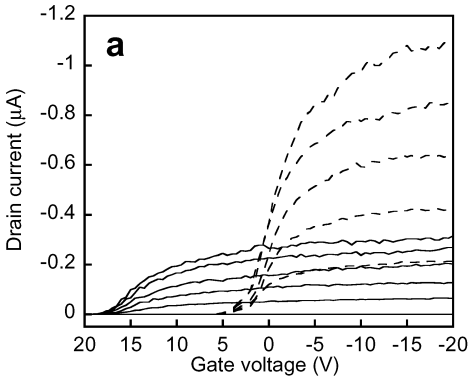

(b) Alcoholic vapor sensor [63]

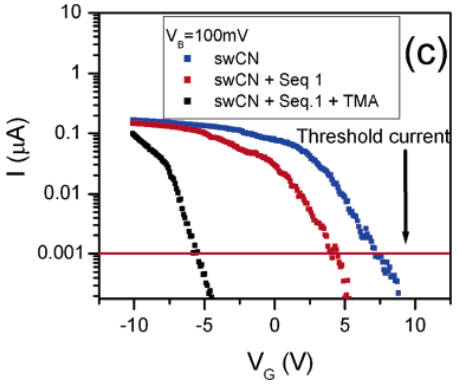

(c) Chemical sensor [64]

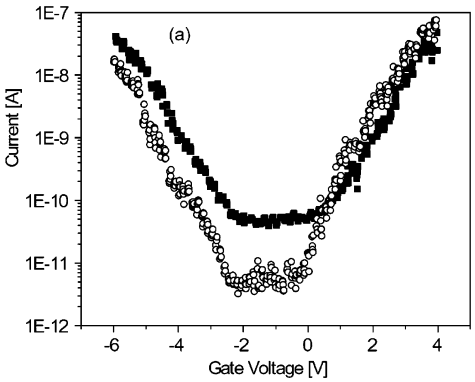

(d) Infrared sensor [65]

Figure 2.22: Transfer characteristics of CNTFETs used in different sensor applications. (a) Gas sensor from [62]; (b) Alcoholic vapor sensor from [63]. Measurement in saturated vapor of ethanol (dash line) and in air (solid line); (c) Chemical sensor from [64]. Blue transfer characteristic: CNTFET with bare SWNT. Red one: DNA-decorated SWNT. Black one: DNA-decorated SWNT exposed to trimethylamine (TMA) vapor; and, (d) Infrared sensor from [65]. Transfer characteristic with circle: measurement in the dark. Characteristic with square: under infrared illumination.

to a horizontal shift of the transfer characteristic, which can be easily detected. Someya et al. report on the use of CNTFET as an alcoholic vapor sensor (see Fig. 2.22b) [63]. Once again, the threshold voltage but also the on-current of the transistors are found to change in an alcoholic vapor environment. The decoration of SWNTs with DNA (deoxyribonucleic acid) to provide a

chemical recognition site is shown to be very promising [64]. Lastly, CNTFETs have been used to measure the chemical potential of a solution [66].

Fig. 2.22 compiles four measurements of CNTFETs used as chemical and infrared sensors: only a horizontal shift in the transfer characteristic proves the presence or absence of the chemical quantity to be detected. All these examples prove that s-SWNT devices are very promising. Working on the improvement of their fabrication is an indispensable topic of research nowadays.

Detection of light based on photoconductivity as well as emission of light (photoemission) are also possible because s-SWNTs are direct semiconductors (see subsection 2.2.4). The photoconductivity of SWNTs was observed for the first time in 2001 in Japan. Fujiwara et al. reported on the photoconductivity of an SWNT network illuminated by a pulsed laser with photon energies between 0.5 and 2.8 eV [67]. The network is composed of a mixture of metallic and semiconducting tubes. In 2003, IBM researchers together with Carbon Nanotechnologies, Inc. researchers reported for the first time on the photoconductivity of a single semiconducting SWNT which acts as the channel in a field-effect transistor (see Fig. 2.22d) [65]. The transistor shows an ambipolar behavior and exhibits different transfer characteristics under infrared illumination or in the dark. The off-current is increased by one order of magnitude under illumination and a quantum efficiency higher than 10% was estimated from the measurements. In the same year, IBM researchers also observed the polarized infrared optical emission from a carbon nanotube ambipolar field-effect transistor [68]. More recently, a paper has been published which demonstrates the feasibility of infrared detectors based on the bolometric infrared photoresponse of SWNTs layers [69]. The film changes its conductivity under infrared illumination due to the heating of SWNTs layers. These detectors are very simple structures because they do not need to be included in FET structures. However, the time response of bolometric sensors is very slow.

2.5 Conclusions and motivation for this PhD work

In this chapter, an attempt has been made to give an overview of carbon nanotubes, especially single-walled carbon nanotubes, which possess numerous promising properties like one-dimensional form, diameter in the nanometer range, ballistic transport, sensor capability and a metallicty which depends on their chirality. The operation of SWNT based field-effect transistors has been summarized, based on the results published by the scientific community on these devices. Indeed, the fabrication of CNTFETs have been reported several times, with different gate configurations and materials. The uses of CNTFETs not only as basic FET but also as diverse sensors has also been demonstrated.

However, in most cases, only single individual devices are fabricated. Data on fabrication process suitability (e.g. time, costs), device reproducibility and reliability or yield are not available. State-of-the-art CNTFETs are mostly only prototypes, often due to the SWNT growth method, i.e., arc discharge or laser ablation, which are not suitable for the simultaneous fabrication of a large number of devices (see next chapter).

Improving the knowledge of the scientific community on the feasibility of a large scale fabrication of carbon nanotube devices constitutes the major motivation of this PhD work. Attendant statistics on yield and reproducibility belong to the major goals as well. This experimental and analytical work should be concluded by a viable statement on the eventual replacement of MOSFETs with CNTFETs in CMOS technology in the future.